

Review

Open Access



Cathode architecture and active site engineering in lithium-CO₂ batteries

Haobo Sun¹, Chuanli Di¹, Zeyi Wu¹, Ying Jiang³, Iftikhar Hussain⁴, Zhengqing Ye^{1,2}

¹Tianjin Key Laboratory of Materials Laminating Fabrication and Interface Control Technology, School of Material Science and Engineering, Hebei University of Technology, Tianjin 300401, China.

²Joint Key Laboratory of the Ministry of Education, Institute of Applied Physics and Materials Engineering, University of Macau, Taipa, Macau SAR 999078, China.

³School of Material Science and Engineering, Tianjin Key Lab of Photoelectric Materials & Devices, Key Laboratory of Display Materials and Photoelectric Devices (Ministry of Education), Tianjin University of Technology, Tianjin 300384, China.

⁴Department of Mechanical Engineering, City University of Hong Kong, Kowloon, Hong Kong.

Correspondence to: Prof. Zhengqing Ye, Tianjin Key Laboratory of Materials Laminating Fabrication and Interface Control Technology, School of Material Science and Engineering, Hebei University of Technology, No. 5340, Xiping Road, Beichen District, Tianjin 300401, China. E-mail: zqye@hebut.edu.cn

How to cite this article: Sun, H.; Di, C.; Wu, Z.; Jiang, Y.; Hussain, I.; Ye, Z. Cathode architecture and active site engineering in lithium-CO₂ batteries. *Microstructures* 2025, 5, 2025014. <https://dx.doi.org/10.20517/microstructures.2024.45>

Received: 11 May 2024 **First Decision:** 16 Jul 2024 **Revised:** 29 Jul 2024 **Accepted:** 14 Sep 2024 **Published:** 14 Feb 2025

Academic Editor: Hailong Chen **Copy Editor:** Fangling Lan **Production Editor:** Fangling Lan

Abstract

Secondary lithium-carbon dioxide (Li-CO₂) batteries possess great application potential for CO₂ fixation and electrochemical energy storage. Nevertheless, the formation of stable and insulating discharge intermediates and the complexity of multiphase interfacial reactions lead to large potential polarization and inferior redox reversibility. In this review, we systematically discuss the charge/discharge mechanisms of Li-CO₂ redox reaction. Latest research achievements about cathode architecture and active site engineering are summarized in detail. In particular, representative engineering strategies (i.e., morphological modulation, dimensional hybridization, defect, single atoms, heterostructure, and synergy engineering) of cathode materials for high-performance Li-CO₂ batteries are systematically introduced. Lastly, the current research progress is briefly summarized and the future challenge and potential opportunities for further development of advanced Li-CO₂ batteries are proposed.

Keywords: Cathode architecture, active site engineering, carbon dioxide conversion, Li-CO₂ batteries



© The Author(s) 2025. **Open Access** This article is licensed under a Creative Commons Attribution 4.0 International License (<https://creativecommons.org/licenses/by/4.0/>), which permits unrestricted use, sharing, adaptation, distribution and reproduction in any medium or format, for any purpose, even commercially, as long as you give appropriate credit to the original author(s) and the source, provide a link to the Creative Commons license, and indicate if changes were made.



INTRODUCTION

Global energy resource depletion has increased significantly, resulting in the energy crisis and greenhouse effect^[1,2]. The exploration for renewable and clean energy is the basic condition for achieving sustainable development. Among them, secondary batteries are recognized as emerging devices for the effective utilization of renewable energy resources^[3-5]. Recently, the increasing popularity of Li-CO₂ batteries, which integrate CO₂ capture with electricity formation without needing electricity input, has aroused widespread research attention^[6-8]. An advanced Li-CO₂ battery device with ultrahigh discharge potential (≈ 2.8 V) and a high theoretical energy density over 1,876 Wh kg⁻¹ has been lately developed to reduce the depletion of fossil resources and fix CO₂, as well as achieve carbon neutrality^[9,10]. Furthermore, Li-CO₂ batteries possess substantial application potential in the aerospace and deep-sea fields. Abundant CO₂ atmosphere offers a significant advantage for the potential application of Li-CO₂ batteries in Mars rovers and deep ocean tasks. In particular, compared with the Li-ion batteries, the Li-CO₂ batteries possess a higher energy density, supporting economical energy storage systems for sustainable energy networks^[7]. Also, the associated electrochemical reaction mechanisms are relatively simple in comparison with Li-O₂ batteries, only involving the electrochemical reduction reaction of CO₂ (CO₂RR) on the cathode surface^[11]. The electrochemical CO₂RR was initially detected by Takechi *et al.* in the Li-O₂/CO₂ battery in 2011^[12]. Subsequently, they demonstrated that with the presence of CO₂, the discharge capacity can significantly increase compared to Li-O₂ batteries. Lately, Xu *et al.* fabricated a Li-CO₂ battery by applying a carbon host in an ionic liquid electrolyte^[13]. Afterward, rechargeable pure Li-CO₂ batteries were rapidly developed by distinctive cathode design and excellent electrolyte formulation to promote the formation and decomposition of insulating Li₂CO₃.

It is worth mentioning that CO₂ electrodes are a crucial part of air-assisted Li-CO₂ devices, playing a significant role in catalyst loading, electron transfer, efficient gas diffusion, and necessary interface barriers^[6,14]. Despite the significant breakthroughs achieved on exploring highly efficient electrocatalysts and architectures of CO₂ electrodes in recent years, some serious issues remain. One of the most challenging problems is to overcome the high reaction energy barriers in Li-CO₂ batteries. The existence of a thermodynamically stable C=O bond in CO₂ molecules results in an endothermic process for CO₂ transformation, which is energetically unfavorable. Furthermore, the involved multielectron/mass transport processes also impede the electrochemical reactions in Li-CO₂ batteries. From this perspective, the rational design of cathode architecture and catalysts plays a crucial role in enhancing reaction kinetics, promoting energy conversion efficiency and accelerating mass transport. However, while great progress was made on exploring highly efficient catalysts, the attention to air electrode architectures for Li-CO₂ batteries was limited^[15,16]. In addition, few reviews have summarized on the active site engineering of electrocatalysts especially their electrochemical reconstruction during cycling in Li-CO₂ batteries^[4].

In this review, we primarily focus on the latest advancements in the cathode structure and active site engineering in Li-CO₂ batteries. To offer a fundamental understanding of the Li-CO₂ batteries, we initially introduce the vital reaction mechanisms of CO₂RR and CO₂ evolution reaction (CO₂ER). Next, advanced structure and active site engineering strategies are detailed, highlighting structure-property relationship for Li-CO₂ batteries including morphological modulation, dimensional hybridization, defect, single atoms, heterostructure and synergy engineering. In particular, identification of the active sites and their reconstruction during cycling in the Li-CO₂ batteries are systematically reviewed. Combined with the recently reported cases for advanced Li-CO₂ batteries, some rational strategies and fundamental rationales for cathode architecture and active site engineering are summarized in detail. Finally, we propose the potential challenges and prospects for the next-generation cathode materials in advanced Li-CO₂ batteries.

MECHANISMS OF LI-CO₂ BATTERIES

Generally, Li-CO₂ batteries consist of both metal lithium anodes and cathode catalysts. During discharge process, CO₂ will undergo complex conversion reactions involving multiple electron/mass transport processes to generate various carbonaceous products [Figure 1A]. The cathode of Li-CO₂ batteries plays a key role in the battery performance, which involves the complex gas-liquid-solid multiphase interfacial reactions. In general, to construct a high electrochemical performance cathode, it is generally necessary to incorporate a minor weight percentage of binder to form a conductive carbon network. The binding agent is usually a thermoplastic polymer such as polyvinylidene fluoride (PVDF) or polytetrafluoroethylene (PTFE), which enables the carbon materials to create a slurry by mixing a non-reactive organic solvent^[7]. This mixture is subsequently cast onto a gas transport current collector and dried to obtain a CO₂ cathode. In particular, the transport of electrons and carbon dioxide is regarded to be the determining step(s) for Li-CO₂ batteries. The nonuniform distribution of pore sizes (micro-, meso-, and macro-pores) contributes differently to transport and reactions. The complex pore connectivity results in uniform channel sizes and transport anisotropy. The straight channels are expected to provide simple and rapid transport pathways of species during the cycling process^[17]. Specifically, CO₂ and Li ions enter the oriented channels, undergo transport, and participate in conversion reactions on the cathode surface [Figure 1B]. While the ordered porous structures offer a conductive pathway for rapid mass transport, the sluggish electron transfer from the electrode to intermediates is induced by the inferior activity of active sites^[18] [Figure 1C]. Thus, designing efficient electrocatalysts that could achieve rapid electron transfer is also needed [Figure 1D]. A significant approach to achieving rapid electron transfer is establishing active site engineering, where the energy band and electronic structure are efficiently regulated. Constructing efficient cathode catalysts with rapid electron transfer and fast mass transport provides a new avenue for high-performance Li-CO₂ batteries. Investigating the intrinsic reaction mechanisms of CO₂ cathodes can significantly facilitate the rational design of advanced Li-CO₂ batteries. In this part, we summarize several different reaction routes of Li-CO₂ electrochemistry and discuss related working mechanism for CO₂RR and CO₂ER in aprotic Li-CO₂ batteries.

Mechanisms of aprotic CO₂RR

During a discharge process, a lithium metal anode provides several electrons and produces lithium ions that are then transported to the CO₂ cathode side. The CO₂RR usually occurs at the gas-liquid-solid interface among CO₂/aprotic electrolyte/electrocatalyst, where the CO₂ is able to be transformed to discharge products, including Li₂CO₃/C, Li₂CO₃/CO, Li₂C₂O₄, and HCOOH, with the involvement of Li⁺ ion and electrons.

The Li₂CO₃/C is generally accepted as a discharge product in rechargeable aprotic Li-CO₂ batteries^[13].



The peroxide-type intermediate could be preferred on carbon-based cathodes. For example, a one-electron reduction of CO₂ generates C₂O₄²⁻ [Figure 2A], resulting in an open circuit potential (3.0 V)^[19]. The intermediate C₂O₄²⁻ disproportionate constantly in the successive two steps [Figure 2A], generating stable crystalline Li₂CO₃. Specifically, the formation of Li₂CO₃/C is impacted by the adsorption energy between intermediates and electrocatalysts [Figure 2B]^[20]. If the binding energy between carbonaceous intermediates and the cathode is relatively weak, the Li₂CO₃ preferentially generates in the aprotic electrolyte close to the CO₂ cathode surface via a solvation-mediated growth process. On the contrary, if a sufficiently strong binding energy exists between the carbonaceous and catalyst surface, the Li₂CO₃ layer is inclined to form directly on CO₂ cathode surface by surface-adsorption interaction to generate homogeneous and conformal microstructure.

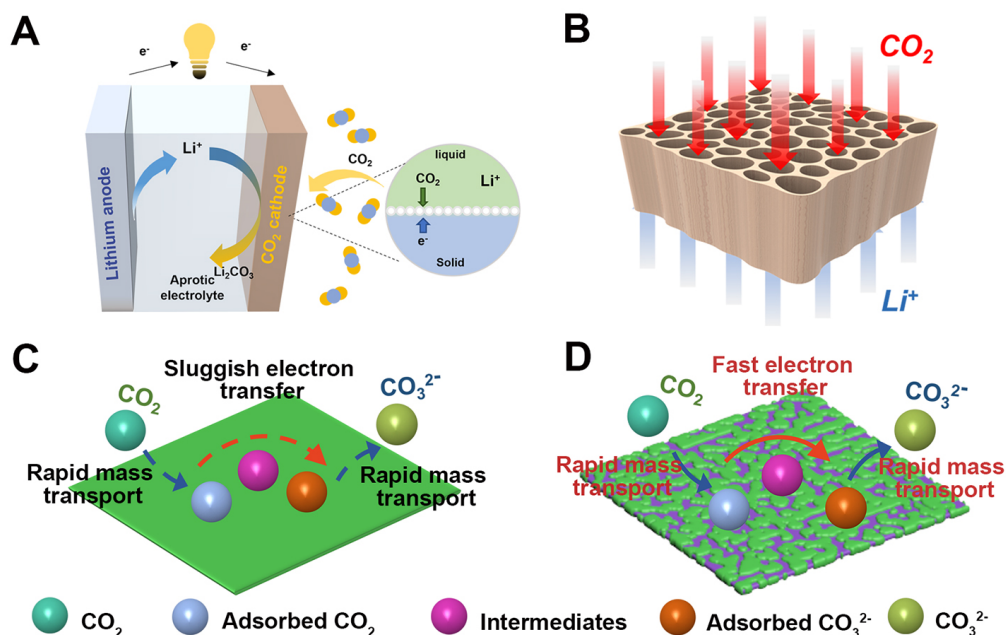


Figure 1. (A) Schematic diagram of Li-CO₂ battery operation. (B) The scheme of mass transport processes in the porous CO₂ cathode. (C and D) Schematic of mass transport and electron transfer in CO₂RR process on various electrocatalyst surfaces.

Another disproportionation reaction occurs in aprotic Li-CO₂ batteries on the basis of Li₂CO₃ and CO, which facilitates batteries with low overpotential and highly reversible [Figure 2C]. In 2013, Xu *et al.* first reported that Li₂C₂O₄ intermediates could be transformed into CO and Li₂CO₃ at high temperatures^[13]. Qiao *et al.* used *in-situ* Raman spectroscopy to observe intermediate evolution during discharge process on an Au substrate^[21]. Li₂CO₃ and C species features can be obviously observed [Figure 2D]. Interestingly, a smaller discharge plateau was monitored at about 1.8 V at 20 μAh. This discharge plateau can also be attributed to the presence of Li₂O species [Figure 2E]. The electrochemical redox reaction was expressed as follows:



The calculated standard electrode potential of 1.89 V refers to the discharge plateau. The low discharge plateau is attributed to the ultralow CO₂ content and dynamic equilibrium on the electrode surface. Nevertheless, Li₂O is inclined to transform into Li₂CO₃ in an atmosphere including CO₂.

Recently, research has reported that thermodynamically unstable Li₂C₂O₄ as the ultimate discharge product can decrease the charge voltage to 3.8 V utilizing specific cathode catalysts in Li-CO₂ batteries^[22,23] (Equation 3).



An oxalate-based (C₂O₄²⁻) pathway is inclined to be promoted by metal-rich cathodes. For example, Li *et al.* analyzed and proved the electrocatalytic CO₂RR via solid redox mediator Cu (II)-MOF (denoted as RM(II)-BTC) during the discharging process^[24]. Firstly, during the process of discharge, solid RM(II)-BTC loaded onto the carbon nanotube (CNT) surface is reduced to low-valence Cu(I)-MOF (denoted as RM(I)-BTC).

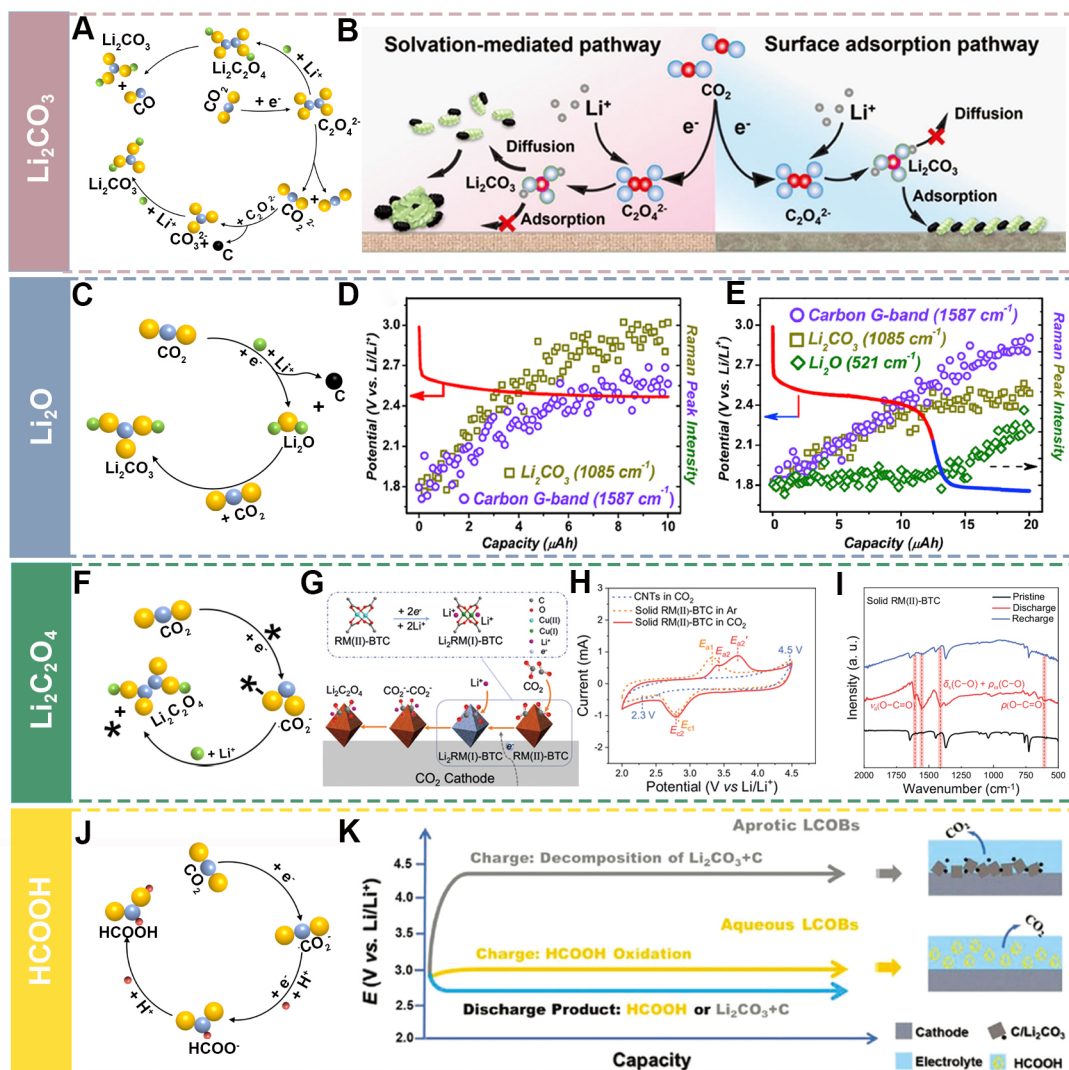


Figure 2. (A) Formation mechanism of Li₂CO₃. (B) Growth mechanisms for Li₂CO₃/C products. (Reproduced with permission^[3]. Copyright 2023, Wiley-VCH). (C) Formation mechanism of Li₂O. (D and E) Galvanostatic discharge curves and corresponding product of the Li-CO₂ battery under different capacities. (Reproduced with permission^[21]. Copyright 2017, Elsevier). (F) Formation mechanism of Li₂C₂O₄. (G) Solid RM(II)-BTC-catalyzed reaction mechanism towards Li₂C₂O₄ pathway. (H) The CV curves of solid RM(II)-BTC and CNTs cathode in CO₂ and Ar atmosphere. (I) Ex-situ FTIR spectra of solid RM(II)-BTC cathode. (Reproduced with permission^[24]. Copyright 2024, Springer Nature). (J) Formation mechanism of HCOOH. (K) Comparison between aqueous and aprotic Li-CO₂ batteries. (Reproduced with permission^[27]. Copyright 2021, Wiley-VCH).

Subsequently, RM(I)-BTC interacts with captured CO₂ to successively generate Cu(II)-CO₂⁻ and Cu(II)-C₂O₄²⁻-Cu(II) intermediates through the chemical reactions. Finally, Li ions combine with the Cu(II)-C₂O₄²⁻-Cu(II) intermediates, evolving Li₂C₂O₄ product on the surface of solid RM(II)-BTC [Figure 2F and G]. Interestingly, solid RM(II)-BTC cathodes show different redox peaks at 3.34 V (E_{a1}) and 2.81 V (E_{c1}), respectively, revealing the reversible oxidation and reduction reaction of Cu(II)/Cu(I) in solid RM(II)-BTC. In comparison with the oxidation peak at (E_{a1}) in Ar atmosphere, two new oxidation peaks occurred in CO₂ atmosphere, resulting from the oxidation of trace Cu(I) (E_{c2}) and corresponding to the decomposition of the Li₂C₂O₄ discharge product, respectively [Figure 2H]. Besides, they found that noticeable characteristic peaks of Li₂C₂O₄ are observed in the discharged cathode by ex-situ Fourier transform infrared (FTIR) spectroscopy [Figure 2I]. Similarly, Wang *et al.* synthesized a soluble redox

mediator (2,2,6,6-tetramethylpiperidoxyl, denoted as TEM RM) to facilitate selective transformation of CO₂ into Li₂C₂O₄ [25]. The soluble TEM RM first combined CO₂ molecules from the electrolyte, generating TEM⁻-Li⁺-CO₂ intermediates that promoted electron transport during the discharge process. Subsequently, the original TEM was liberated and Li₂C₂O₄ layers were precipitated regularly, which improves the redox kinetics and rechargeability. Moreover, the donor number (DN) of solvents also possesses a significant impact on the discharge process. In high-DN solvents, the generation of reaction intermediates (C₂O₄²⁻ and C₂O₆²⁻) in Li-CO₂ batteries proceeded mainly by an “electrochemical solution pathway (high capacity but poor stability)”. In contrast, peroxide-type intermediate (Li₂O₂) reacted with CO₂ to generate Li₂CO₃ by a “chemical surface pathway (low capacity but high stability)” in low-DN solvents [26].

Apart from solid discharge products, soluble liquid-phase products could be optimal because they can efficiently desorb from the active site, and adequate contact between catalysts and intermediates ensures completed decomposition. In particular, formic acid (HCOOH) is appealing and practical due to its high kinetical accessibility. For example, Xue *et al.* employed a Li_{1+x}Al_xGe_{2-x}(PO₄)₃ (LAGP) as the separator which only provides the transport of lithium ions [27]. They found that Pd substrates served as cathode electrocatalysts for Li-CO₂ batteries (Equation 3) in which potential for HCOOH formation and dissolution is 2.80 V [Figure 2J]. As a result, HCOOH was observed with excellent selectivity and thus active sites are efficiently exposed on the surface of electrocatalysts. The Li-CO₂ battery delivered excellent cycling stability over 300 h with a lower charging voltage (2.99 V).



The Pd with LAGP can facilitate the CO₂RR in the aqueous electrolyte system without impacting the lithium-ion deposition and strip at lithium metal anodes [Figure 2K]. During discharging process, metallic Li releases electrons and the produced Li⁺ ions are transported across the LAGP separator, resulting in the formation of HCOOH from CO₂ on cathodic Pd films. Nevertheless, side reactions, such as CO evolution reaction (COER) and hydrogen evolution reaction (HER), can decrease selectivity and induce catalyst degradation. In addition, the local pH alteration during electrocatalysis process resulted from the depletion of protons or the generation of OH⁻, which could influence the HCOOH selectivity [28].

Mechanisms of CO₂ER

Theoretically, CO₂ER during charge possesses can be regarded as the reverse reaction of CO₂RR, in which CO₂ at the cathode side and metallic Li at the anode side are respectively regenerated [Figure 3A]. As a typical example, Qiao *et al.* found that the discharging voltage plateau of Ru-based cathode [Figure 3B] presented an obvious decrease compared with Au-based cathodes [21]. The reduction of both carbon species and Li₂CO₃ content was detected on the metal Ru substrate [Figure 3C], revealing that the dissolution of both discharge intermediates with the metal Ru catalyst occurred via a one-step reaction as follows:



In contrast, the characteristic peaks of carbon species remain unchanged in Au-based Li-CO₂ batteries through *in-situ* Raman, indicating that Au-based catalysts only allow the self-decomposition of Li₂CO₃ [Figure 3D]. Furthermore, they proposed the specific charging products of oxygen species at the corresponding discharge-charge stages [Figure 3E and F]. Differential electrochemical mass spectrometry (DEMS) measurements indicated that the solo decomposition of Li₂CO₃ at a low current density followed the reaction step [Figure 3G]:

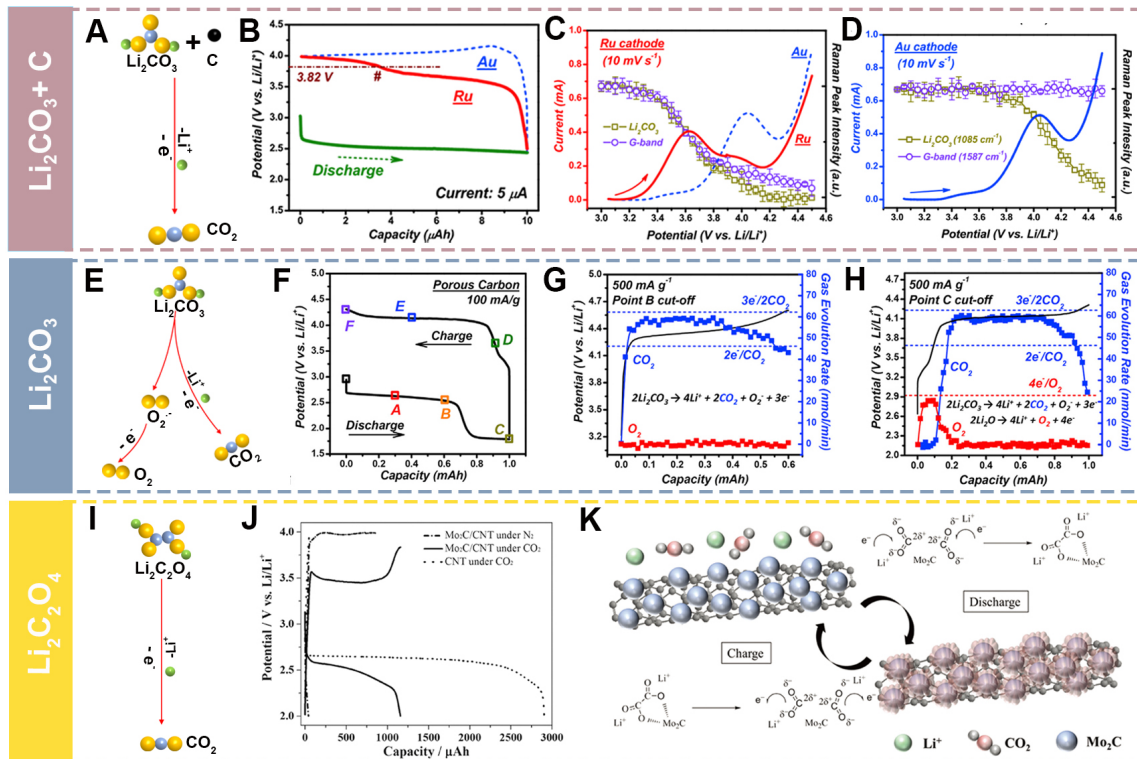


Figure 3. (A) Decomposition mechanism of $\text{Li}_2\text{CO}_3/\text{C}$. (B) Galvanostatic charge/discharge profile of the Ru/Au-based cathode. Linear potential scan curves at both the Ru (C) and Au (D) cathodes. (E) Decomposition mechanism of Li_2CO_3 . (F) Voltage profile of a Li- CO_2 battery. (G) The DEMS figures of discharging to point-B and (H) discharging to point-C. (Reproduced with permission^[21]. Copyright 2017, Elsevier). (I) Decomposition mechanism of $\text{Li}_2\text{C}_2\text{O}_4$. (J) Galvanostatic charge-discharge profiles of different electrodes. (K) Schematic diagram of reactions during charge and discharge of $\text{Mo}_2\text{C}/\text{CNT}$. (Reproduced with permission^[29]. Copyright 2017, Wiley-VCH).



Increasing the battery capacity limitation to the discharge plateau of Li_2O (1.0 mAh), the emergence of O_2 was detected [Figure 3H]. Moreover, according to the obtained charge-to-mass ratio of $4\text{e}^-/\text{O}_2$ at the specific stage, the solo dissolution mechanism of the Li_2O ($2\text{Li}_2\text{O} \rightarrow \text{O}_2 + 4\text{Li}^+ + 4\text{e}^-$) could be further affirmed.

In addition to Li_2CO_3 and $\text{Li}_2\text{CO}_3/\text{C}$, Hou *et al.* proposed that charging products of $\text{Li}_2\text{C}_2\text{O}_4$ in $\text{Mo}_2\text{C}/\text{CNT}$ -based Li- CO_2 batteries [Figure 3I]^[29]. In contrast to CNT-based cathodes, the amorphous $\text{Li}_2\text{C}_2\text{O}_4$ - Mo_2C discharge product can be decomposed below 3.5 V on charge [Figure 3J]. The Mo_2C possesses stabilization function owing to the low valence of Mo in Mo_2C , which facilitates the transport of outer electrons to oxygen within $\text{Li}_2\text{C}_2\text{O}_4$ intermediate product and impedes its disproportionation to Li_2CO_3 . Subsequently, only the amorphous $\text{Li}_2\text{C}_2\text{O}_4$ - Mo_2C liberates CO_2 and Li^+ below 3.5 V during charging process [Figure 3K]. Consequently, Mo_2C is expected to play a crucial role in stabilizing $\text{C}_2\text{O}_4^{2-}$ species and prevent its subsequent disproportionation reaction.

In addition, it has been demonstrated that metal-based cathodes could stabilize the intermediate $\text{Li}_2\text{C}_2\text{O}_4$ using cobalt phthalocyanine and copper complex mediators^[18,22]. Moreover, researchers have not yet elucidated the dissolution mechanisms of other reaction intermediates, such as HCOOH . More investigations are required to explore the reversibility and rechargeability of Li- CO_2 batteries.

MORPHOLOGICAL MODULATION

Shaped nanomaterials

Electrode materials can exhibit greatly enhanced electrochemical properties after reducing their sizes, since the nanoscale effect often renders these materials with higher electronic conductivity and robust structural stability^[11,23]. The nanoscale materials are anticipated to promote the round-trip conversion of CO₂RR and CO₂ER. Because of different synthetic methods, these nanosized materials usually display various shapes, such as spheres, polyhedrons, nanosheets, and nanorods. In this section, we discuss the rational design and potential applications of these shaped nanoparticles in Li-CO₂ batteries by utilizing typical instances of nanosheets and nanorods.

The 1D materials with interconnected fibrous networks are demonstrated to afford favoring pathways for rapid electron transfer and enhance interface interaction between fiber supports and electrolytes^[30,31]. Besides, many functional modifiers are added into these 1D fibrous substrates including nanotubes^[32], nanofibers^[33], and nanorods^[34] to improve their overall characteristics, such as reaction intermediates and electrocatalysts.

In terms of study of fibrous-based materials for Li-CO₂ batteries, a representative example is one in which Zhou *et al.* successfully synthesized unusual phase 4H/fcc Ir microstructures by the formation of Ir on the surface of 4H/fcc Au nanorods [Figure 4A and B]^[35]. High-angle annular dark field scanning transmission electron microscopy (HAADF-STEM) technique revealed that 4H and fcc phases were clearly observed [marked regions of Figure 4C]. Furthermore, after the first discharge state, large-sized aggregates of discharge products were dispersedly distributed in the Au cathode; in contrast, the discharge products existed in the form of a continuous thin film covering electrocatalysts in the Au@4H/fcc-Ir_{0.14} cathode [Figure 4D]. As a result, 4H/fcc Ir showed superior electrochemical performance than fcc Ir in enhancing the cyclic redox kinetics of CO₂, realizing a low charging plateau below 3.61 V and excellent energy efficiency of 83.8%. The as-fabricated pouch cell can deliver practical cycling stability for a clock even under all kinds of bending angles [Figure 4E]. *In-situ/ex-situ* tests and theoretical calculations indicated that the improved reaction kinetics attributed to the highly reversible formation of low-crystalline discharge products on the surface of 4H/fcc Ir through the Ir-O coupling effect.

In addition to 1D nanomaterials, 2D materials such as graphene, noble metal alloy, transition metal dichalcogenides, and MXene have displayed promising application prospects in Li-CO₂ batteries because of their unique structures and electronic properties^[9,36-43]. As a typical example, a kind of 2D triangular RuRh alloy was synthesized as a bifunctional electrocatalyst for tremendously accelerating the CO₂RR and CO₂ER and realizing excellent performances of Li-CO₂ batteries [Figure 4F]^[44]. The scanning electron microscopy (SEM) images exhibited that the Li₂CO₃ discharge products regularly grew on the RuRh/VC72 surface and reduced in size with improving current density. Nevertheless, Li₂CO₃ particles cannot adequately covered on the VC72 cathode surface at large current density, leading to obviously decreased capacity. Projected density of states (PDOS) calculation revealed that the 4d band exhibits more electron-rich at the Ru-db active sites with 2.2 eV lower than that of the Ru-sf active sites. The Ru-sf sites function as an “electron-depleting center” to facilitate the electron transport toward the adsorbing species. Experiments and calculations revealed that ultrathin RuRh alloy nanosheets are able to not only significantly promote Li₂CO₃ decomposition but also act as the bifunctional active sites for CO₂RR and Li₂CO₃ nucleation. As a result, the RuRh-based Li-CO₂ battery delivered the smallest potential gap (1.35 V) during the discharge-charge process and long cycle life (180 cycles) with a limited capacity of 1,000 mAh g⁻¹ at 1,000 mA g⁻¹ [Figure 4G].

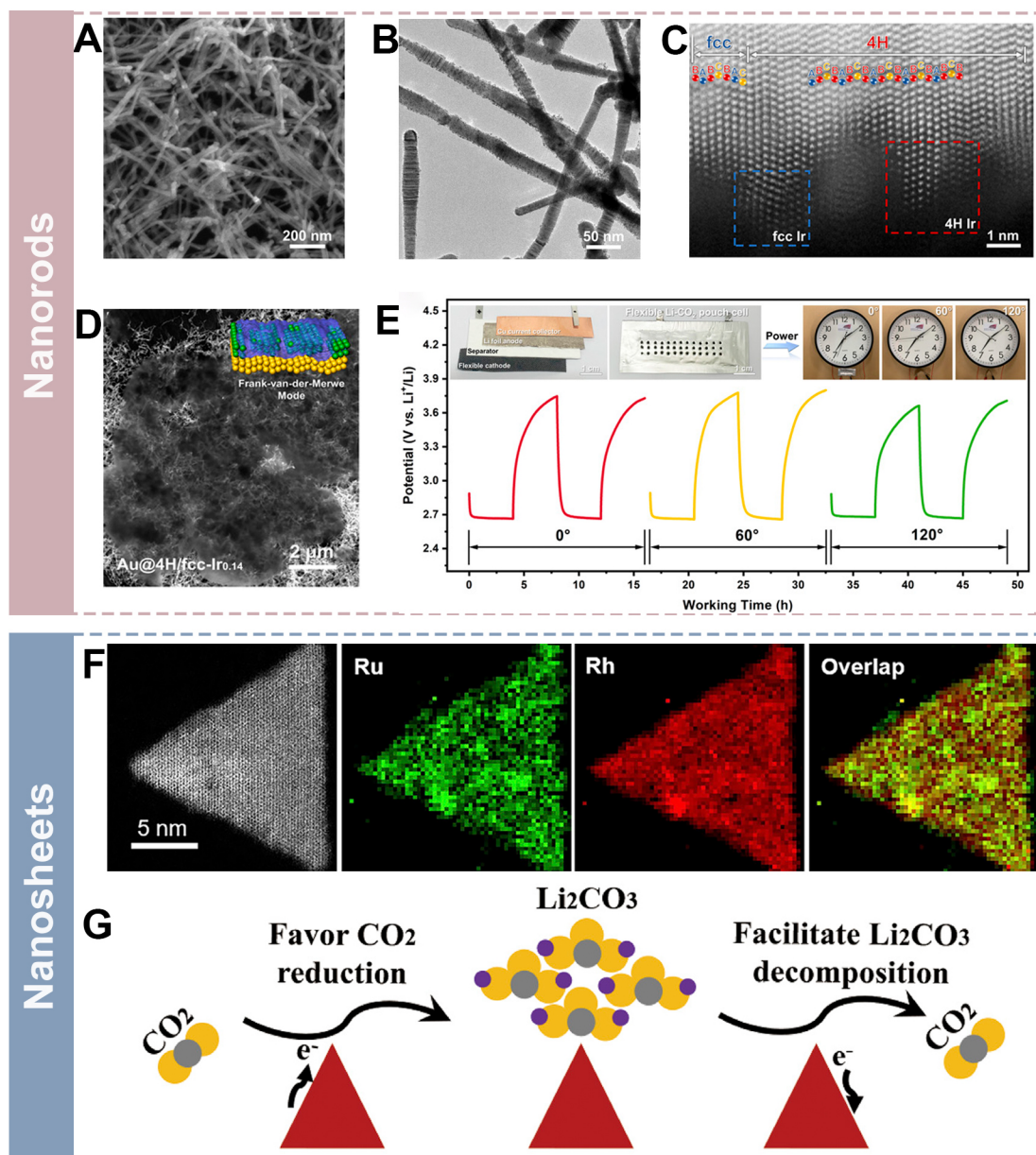


Figure 4. (A) SEM, (B) TEM and (C) HAADF-STEM images of the as-synthesized Au@4H/fcc-Ir_{0.14} nanostructures. (D) SEM images of discharge products generated from the Au@4H/fcc-Ir_{0.14}. (E) Discharge-charge profiles of a Li-CO₂ pouch cell utilizing Au@4H/fcc-Ir_{0.14} (Reproduced with permission^[35]. Copyright 2022, National Academy of Sciences of the United States of America). (F) STEM-EELS elemental mapping of triangular RuRh nanosheet. (G) Schematic Illustration of the reaction mechanism on a single triangular RuRh alloy nanosheet. (Reproduced with permission^[44]. Copyright 2020, Cell Press).

Porous framework

Organic crystal materials with elaborately designed porous structures and versatile sites, including hydrogen-bonded organic frameworks (HOFs), covalent-organic frameworks (COFs), and metal-organic frameworks (MOFs), offer opportunity for the development of high-performance Li-CO₂ batteries^[45,46]. Their functional porous architecture can generate strong binding with CO₂ and O₂. In addition, binding near the catalytic site can effectively enhance the electrocatalytic efficiency. The pore size of organic frameworks can not only satisfy the fast transport of CO₂, aprotic electrolyte and the reaction intermediate

species, but also satisfy the requirement that the proper distance between adsorption and electrocatalytic sites, which should choose the various ligands to improve the pore size to enhance the catalytic efficiency. Therefore, the unique advantages of a porous framework are shorter diffusion pathways, easier near active sites for conversion reactions, and various functionalized inorganic components.

In 2018, Li *et al.* utilized MOFs as an electrocatalyst of the cathode for aprotic Li-CO₂ batteries^[47]. Various nonporous and porous MOFs were investigated in the Li-CO₂ batteries. Experiment results demonstrated that the MOFs with Mn sites can tremendously decrease the charging overpotential, and the great CO₂ absorption ability of MOFs tends to enhance the discharge ability [Figure 5A-C]. *In-situ* DEMS results demonstrated that only CO₂ was formed in a Mn₂(bodbc) cathode during the recharging process, which further indicated the reversible reactions of CO₂ conversion on the MOFs. Recently, the phthalocyanine-based MOF nanosheets (CoPc-Mn-O) have been prepared via the construction of Mn and Co-phthalocyanine, which can act as photocathode catalysts toward light-assisted Li-CO₂ batteries^[48]. Density functional theory (DFT) calculations and advanced characterizations confirmed that the existence of photosensitive CoPc-Mn-O with double metal active sites is conducive to both the CO₂ER and CO₂RR processes under light-assisted condition. The resulting battery delivered a large round-trip efficiency (98.5%) with a very low overpotential (0.05 V) and excellent cycling performance (81.3%) for 60 h at a current density of 0.02 mA cm⁻².

Recently, researchers found that the COFs composed of an electron donor and electron acceptor can improve the electron efficiency and promote the transport of the intermolecular charge-electron^[19]. As a typical example, a porphyrin-based COF (TTCOF-Mn) prepared through the covalent interaction between the electron-donating tetrathiafulvalene (TTF) and electron-accepting tetrakis (4-aminophenyl)-porphyrato manganese(II) (TAPP-Mn) was fabricated as a high-efficiency cathode catalyst for Li-CO₂ batteries [Figure 5D]^[49]. The unique characteristics of TTCOF-Mn consisting of uniform single-Mn(II)-sites, rapid Li⁺ transfer pathways, and excellent electron transport efficiency are beneficial to excellent stability of 180 cycles at 300 mA g⁻¹ with a limited 1,000 mAh g⁻¹ capacity [Figure 5E]. The TAPP-Mn site showed a stronger binding capability toward CO₂ during the aprotic CO₂RR than other metal sites [Figure 5F]. DFT calculations indicated that Pathway 1 is the most thermodynamically favorable among the three possible reaction pathways [Figure 5G]. Huang *et al.* prepared the graphene@COF by uniformly coating graphene with imine COF, using it as a CO₂ catalyst for Li-CO₂ batteries^[50]. CO₂ can be confined in the micropores structures of the imine-COF which can optimize the diffusion pathway of CO₂ and improve the conductivity of electrons and Li⁺. Besides, the regular structure frameworks of COFs can avoid the accumulation and agglomeration of discharge products resulting from high CO₂ concentrations. Moreover, Li *et al.* synthesized a composite material via hybridizing hydrazine-linked COF and CNT covered with Ru nanoparticles (COF-Ru@CNT) as a high CO₂ efficiency catalyst^[51]. The COFs can significantly enhance the capacity of capturing CO₂ in discharge process and accelerate the decomposition of product during recharging. In addition, the stable 1D channels in the COF can be utilized as channels for CO₂⁻ and Li⁺ diffusion and facilitate the kinetics of electrochemical reactions, thereby improving the rate capability. Consequently, the Li-CO₂ batteries delivered an excellent rate capability and operated steadily for 200 cycles at 1,000 mA g⁻¹.

HOFs are generated through hydrogen bonding between organic molecules, which has the benefits of mild preparation processes, low cost and recyclability. Therefore, HOFs hold promising high-efficiency cathodes of rechargeable batteries^[13,21,27,52]. Very recently, the robust HOF (HOF-FJU-1) [Figure 5H] is generated via self-assembly of 3,3',6,6'-tetracyano-9,9'-bicarbazole and serve as a CO₂ cathode via composing with RuO nanoparticle-modified CNT (Ru@CNT)^[53]. The adsorption energies of lithium ions and

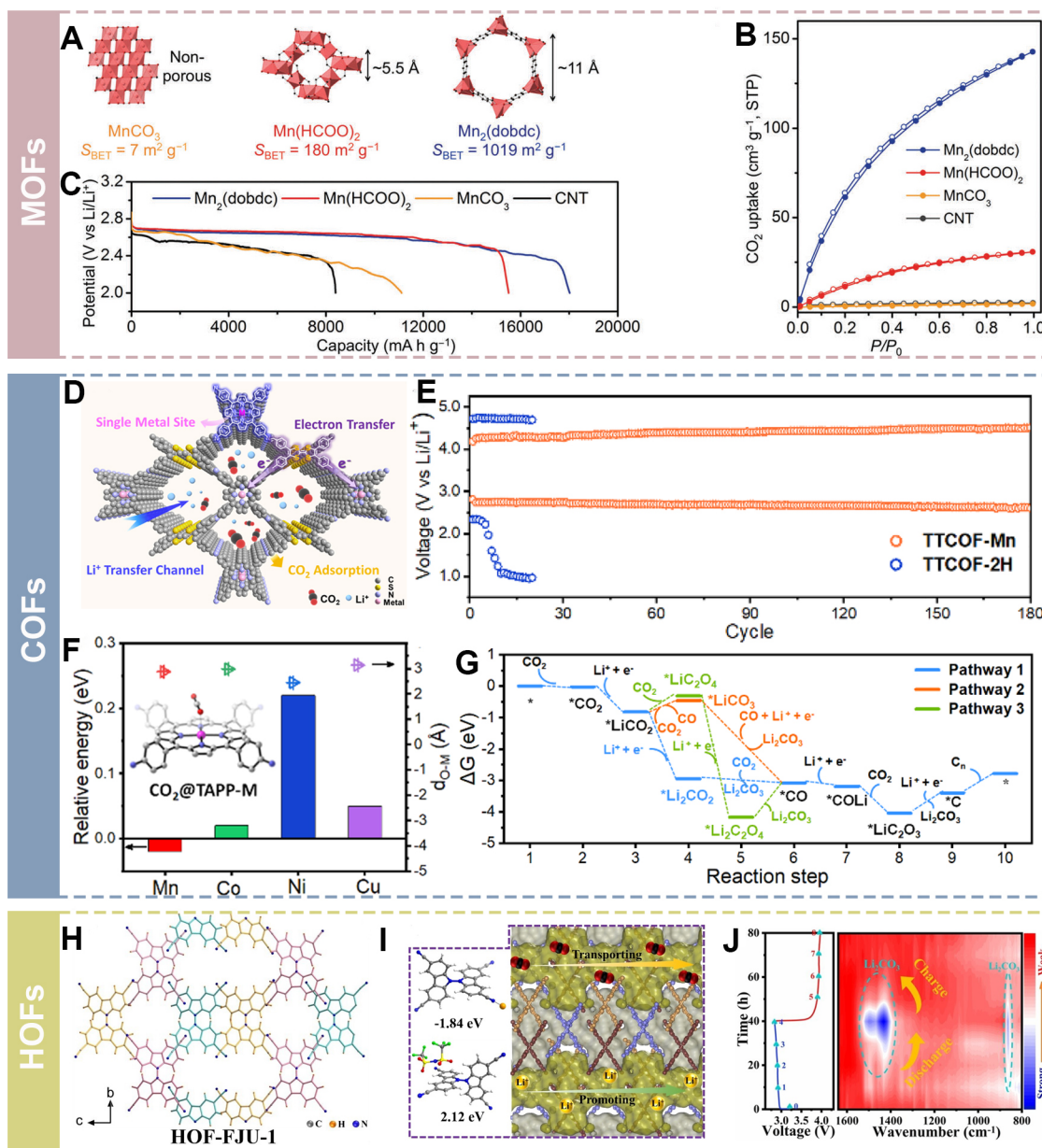


Figure 5. (A) Crystal structures (B) CO_2 adsorption isotherms at a temperature 298 K, and (C) discharge voltage curve at 50 mA g^{-1} with a limited voltage of 2.0 V of different MOF samples (Reproduced with permission^[47]). Copyright 2018, The Royal Society of Chemistry). (D) Illustration of the TTCOF-2H catalysts in Li- CO_2 batteries. (E) Long-term cycling stability of different cathode catalysts at 300 mA g^{-1} . (F) CO_2 binding energy on TAPP-M (M = Cu, Ni, Co, Mn) molecules. (G) Free energy profiles (ΔG) for Li_2CO_3 nucleation and C_n generation with the different reaction pathways on the TAPP-Mn molecule at $U = 0 \text{ V}$ (Reproduced with permission^[49]). Copyright 2021, American Chemical Society). (H) Crystal texture of HOF-FJU-1. (I) Adsorption energies for Li^+ and TFSI^- with HOF-FJU-1, and schematic illustration of CO_2 and Li^+ . (J) *Ex-situ* FTIR spectra of HOF-FJU-1 based cathode (Reproduced with permission^[53]). Copyright 2023, Wiley-VCH).

bis[(trifluoromethyl)sulfonyl]imide anions (TFSI⁻) on the surface of HOF-FJU-1 were -1.84 and 2.12 eV, revealing that HOF-FJU-1 has a stronger attraction to lithium ions and repels TFSI⁻ [Figure 5I]. In addition, the production and dissociation of Li_2CO_3 on the surface of HOF-FJU-1-Ru@CNT catalyst during the charge/discharge were detected by the *ex-situ* FTIR spectrum [Figure 5J], revealing the reversible behavior and dissociation of Li_2CO_3 during charge/discharge. The HOF-FJU-1 with regularly arranged open channels

is helpful for CO₂ and Li⁺ transmission, realizing fast redox kinetic conversion of CO₂. Thus, the Li-CO₂ batteries with HOFs can operate stably at 400 mA g⁻¹ for 1,800 h and remain a small overpotential (1.96 V) at a high current density of 5 A g⁻¹. Despite these promising benefits, the development of HOFs for high-efficiency cathodes in advanced Li-CO₂ batteries has rarely been reported.

DIMENSIONAL HYBRIDIZATION

0D-1D hybridization

Generally, 0D components applied in CO₂ cathodes refer to ultrafine adsorptive/electrocatalytic nanoparticles and even much smaller clusters/single atoms in support materials^[54,55]. Thus, a typical hybridization form of 0D-1D is loading of nanoscale catalysts onto 1D fibrous networks, including nanotubes^[56,57], nanofibers^[58,59] and nanowires^[60]. These nanosized catalysts can expose ample active sites to facilitate the transformation of intermediates; meanwhile, those carbon fibers can offer rapid electron transport pathways and substantial accommodation space for CO₂ species. In this regard, W₂C nanoparticles supported by CNTs (W₂C-CNTs) are successfully synthesized using a two-step carburization approach [Figure 6A and B]^[61]. In comparison with the pure CNTs, the Li-CO₂ battery catalyzed by W₂C-CNTs displayed a large discharge capacity (10,632 mAh g⁻¹) and low polarization voltage [Figure 6C]. The small polarization results from electron-rich W atoms, which break the stable triangle of CO₃²⁻ through W-O bonds [Figure 6D].

Apart from CNTs, the nanofiber is also a promising alternative to 1D skeletal support for embedding of 0D units, which often serves as a substrate to construct flexible freestanding electrodes^[59-62]. For example, Cheng *et al.* reported a bifunctional Mo₂N-ZrO₂ heterostructure in conductive self-standing carbon nanofibers (Mo₂N-ZrO₂@NCNF)^[58]. The Mo₂N-ZrO₂ nanoparticles in conductive carbon nanofibers possess efficient catalytic transformation ability for CO₂ (ZrO₂) and stabilizing performance toward Li₂C₂O₄ (Mo₂N), which simultaneously facilitate CO₂RR and CO₂ER. Therefore, the as-synthesized Li-CO₂ batteries could realize a small overpotential (0.32 V), an ultrahigh energy efficiency (89.8%), and excellent cyclic performance over 400 cycles even at a large current density of 50 μA cm⁻². With synergistic effect by such a 0D-1D hybridization strategy, an optimal 1D construction with interlinked architectures would be constructed, which will undoubtedly enhance the Li-CO₂ battery performance. In the future research, many other 0D-1D interlinked architectures are expected to be studied as CO₂ cathode materials for Li-CO₂ batteries.

0D-2D hybridization

The aforementioned 0D nanomaterials can also interact with 2D support materials, such as MXenes^[63], carbon nanosheets^[64,65], and graphene^[66,67]. As a superior 2D material, graphene is often deployed as a desirable 2D template or skeleton to construct the 0D-2D hybridization materials. For instance, tiny-sized ZnS quantum dots (≈2.5 nm) were synthesized successfully and anchored on the surface of N-doped reduced graphene oxide (ZnS QDs/N-r GO) as a CO₂ host for Li-CO₂ batteries^[67]. It should be mentioned that the electronegative ZnS QDs can offer a large amount of growth sites for discharge products owing to their high CO₂ binding energy and rapid electron transfer, leading to the generation of a thin Li₂CO₃/C layer on the catalyst surface. The average charge potential of Li-CO₂ batteries with ZnS-based catalyst increases to 4.40 V rapidly, while the one with ZnS QDs/N-r GO merely rises from 4.13 to 4.26 V after 190 cycles, indicating excellent catalytic activities and stability for ZnS QDs/N-r GO.

Except for natural 2D graphene, carbon nanosheets can also be easily prepared by rational chemical fabrication methods to serve as a substrate of 0D materials. Recently, Wang *et al.* designed a heterostructure with Te atomic clusters embedded with N-doped carbon nanosheets (TeAC@NCNS)^[68]. Distinct from

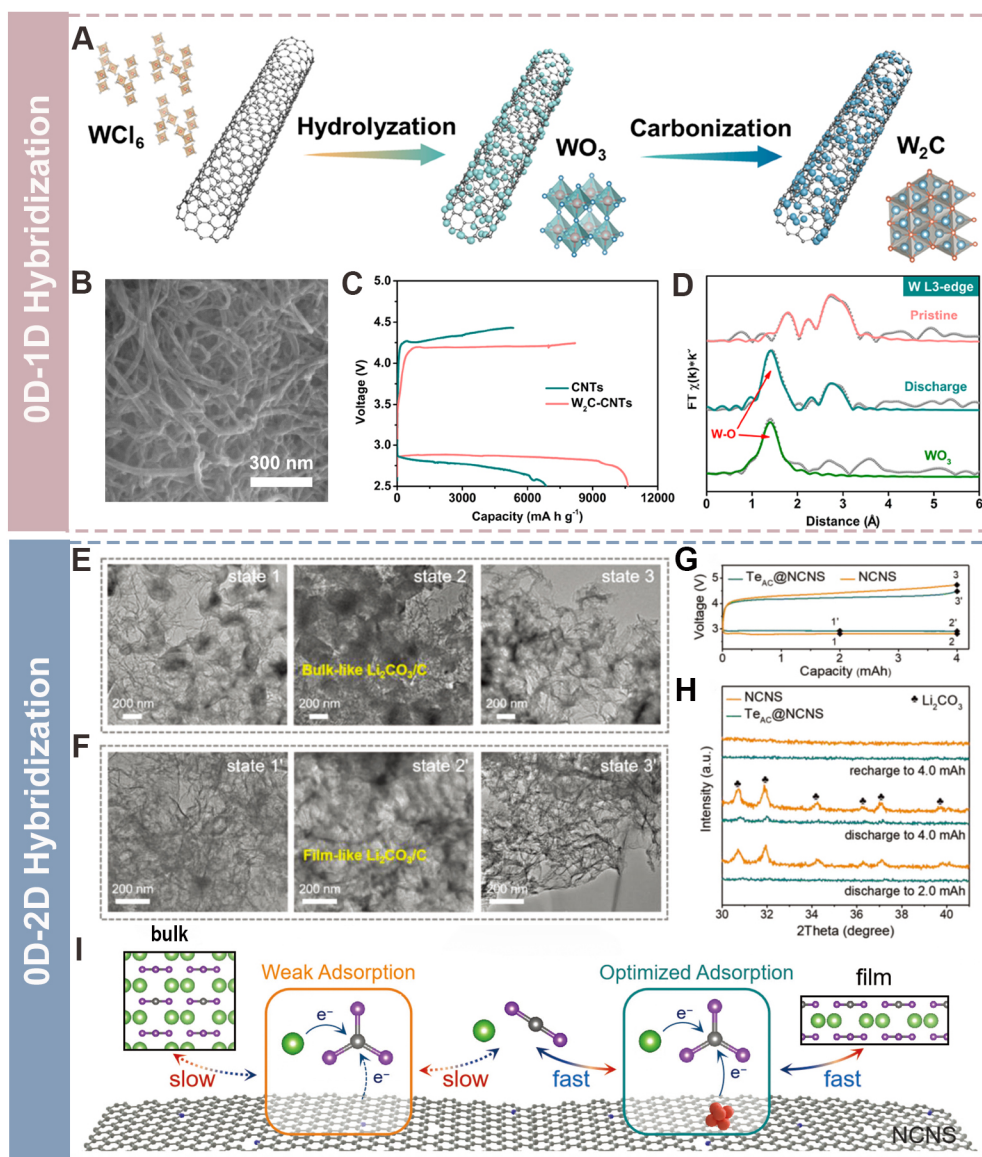


Figure 6. (A) Schematic illustration of synthesis process of the W_2C -CNTs. (B) SEM image of W_2C -CNTs. (C) Deep discharge-charge curves of CNTs and W_2C -CNTs. (D) W_{L3} -edge EXAFS spectra for W_2C -CNTs. (Reproduced with permission^[61]. Copyright 2021, American Chemical Society). TEM images of NCNS (E) and TeAC@NCNS (F) cathodes at different charge and discharge states. (G) Typical first charge-discharge curves of Li- CO_2 batteries. (H) Corresponding *ex-situ* XRD patterns at distinct discharge and charge states. (I) Schematic Illustration of reaction mechanism on multiple catalysts. (Reproduced with permission^[68]. Copyright 2023, Wiley-VCH).

N-doped carbon nanosheets (NCNS) cathodes, high-area and amorphous discharge products are produced on the TeAC@NCNS cathode surface during the discharge process [Figure 6E and F]. Specifically, on the NCNS cathode, some bulk-like discharge product is discretely distributed on the surface of the electrode after discharging the battery to 2 mAh (state 1). Meanwhile, the NCNS nanosheet architecture can still be observed. It was further discharged to 4 mAh (state 2); the densely stacked discharge product fully covered the electrocatalyst surface. A minor number of discharge products remain on the nanosheet surface after recharging (state 3). On the contrary, for the TeAC@NCNS cathode, the film-like discharge products were homogeneously covered on the cathode surface (state 1'). On subsequent discharge to 4 mAh (state 2'), it is

easy to observe the larger-area film-like morphology along the nanosheets. The adequate contact interface between catalysts and discharge products can fully utilize the active sites of TeAC@NCNS, ensuring that the charging process was energetically more favorable. Furthermore, distinct diffraction peaks of Li_2CO_3 species were observed on the NCNS cathode discharged to 2.0 mAh [Figure 6G and H]. Meanwhile, for the TeAC@NCNS cathode, no peaks related to Li_2CO_3 could be detected under the same measurement conditions, indicating the amorphous characteristic of the final discharge product. The TeAC@NCNS cathode with Te atomic clusters provided more CO_2 catalytic sites and enhanced CO_2 RR kinetics. Such a uniformly distributed Li_2CO_3 film can be easily decomposed by a Te atomic cluster catalyst, significantly facilitating Li_2CO_3 decomposition kinetics [Figure 6I]. The as-fabricated battery exhibited an ultrahigh discharge capacity ($28.35 \text{ mAh cm}^{-2}$ at 0.05 mA cm^{-2}) and excellent cycling performance (1,000 h at an ultrahigh cut-off capacity of 1 mAh cm^{-2}).

0D-3D hybridization

In comparison with 0D-1D and 0D-2D hybridization, more 3D nanomaterials can be chosen as supports of 0D materials for the 0D-3D hybridization model because of their unique 3D nanostructured frameworks^[69]. For example, Hu *et al.* successfully anchored single Fe atoms into a 3D N, S-co-doped holey graphene architecture (Fe-ISA/N, S-HG) by a balanced force between the π - π stacking of oxidized holey graphene (HGO) nanosheets and repulsion interaction of their negative charge carboxylate group [Figure 7A]^[70]. The synthesized Fe-ISA/N, S-HG catalyst, with its ample surface area and sufficient space within the crisscrossing holey graphene (HG) network, can not only promote electron transfer and CO_2 /lithium-ion transport, but also realize high uptake of Li_2CO_3 to deliver a large capacity. In addition, its excellent catalytic activity and the absence of Fe single-atom aggregation after cycling result in the generation of small dense Li_2CO_3 nanoparticles loading on the Fe-ISA/N, S-HG electrocatalyst, which can be rapidly dissolved during the charge process [Figure 7B and C]. Consequently, Li- CO_2 batteries with Fe-ISA/N, S-HG cathode showed a high discharge capacity ($23,174 \text{ mAh g}^{-1}_{\text{Fe-ISA/N, S-HG}}$), low voltage polarization (1.17 V at 100 mA g^{-1}), superior rate capability and cycling performance even at a high current density of 1.0 A g^{-1} [Figure 7D].

In addition to HG, the cellulose carbon aerogel (CCA), graphene aerogel^[71], and porous carbon foam^[72] are also promising alternatives to 3D skeletons for embedding of 0D units^[73]. A typical case study by Liu *et al.* successfully synthesized a 3D free-standing CCA with elaborately designed Ru/C heterointerfaces (Ru@CCA) as a promising CO_2 cathode^[74]. The CCA support can offer a rapid mass (Li^+ , CO_2 , *etc.*) and electron transport path and, meanwhile, avoid the loss of active sites induced by stacking of carbon-based substrates. Furthermore, due to the reduced reaction barrier of reaction intermediates and the excellent electronic configuration, the interface of Ru/C exhibited the optimal electrocatalytic activity for CO_2 ER and CO_2 RR during charge-discharge processes. Consequently, the as-obtained Li- CO_2 batteries significantly enhance energy efficiency to 80% with an ultrahigh discharge capacity ($10.71 \text{ mAh cm}^{-2}$ at $20 \mu\text{A cm}^{-2}$) and long cyclic performance (421 cycles at $100 \mu\text{A cm}^{-2}$). These works offer guidelines for the rational design of electrocatalysts with excellent catalytic activity and stability for advanced Li- CO_2 batteries.

1D-2D hybridization

Compared with 0D-3D nanomaterials, the specific surface area of 1D-2D nanomaterials is larger, leading to an ultrahigh density of active sites. These advantages ensure the 1D-2D structure to possess a better synergistic effect^[75]. For example, a novel composite of 2D nanosheet NiO distributed on CNTs was synthesized by a solvothermal approach^[76]. The composite served as a high-efficiency CO_2 cathode electrocatalyst with ultrahigh coulombic efficiency (97.8%) and excellent cycling performance (40 cycles). The NiO-CNT with highly covered NiO nanosheets on CNTs can offer superior electrocatalytic activity sites for the dissolution of product Li_2CO_3 during charging process.

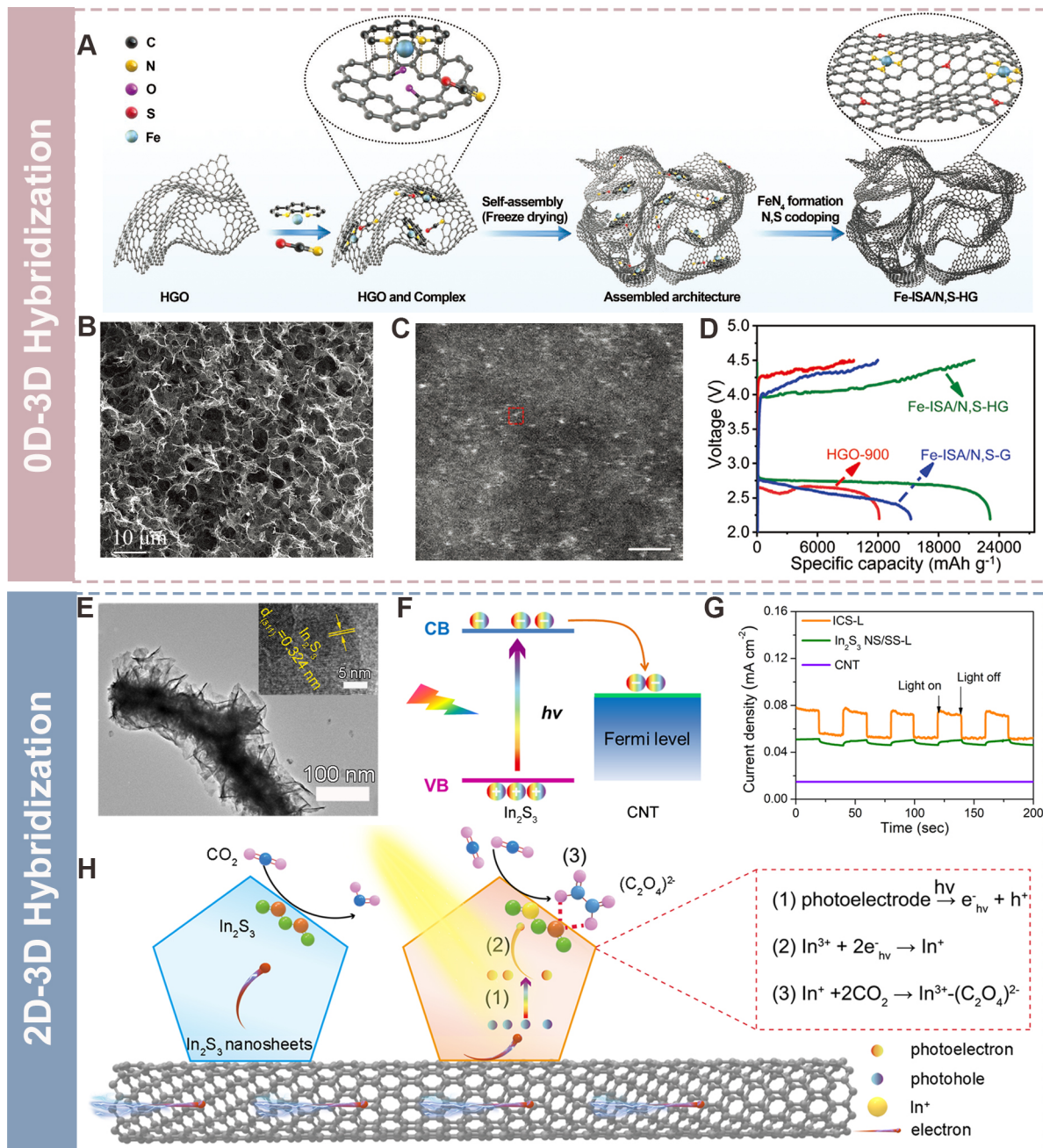


Figure 7. (A) Schematic illustration of the synthesis process of Fe-ISA/N, S-HG. (B) SEM and (C) Atomic-resolution STEM images of Fe-ISA/N, S-HG. (D) Full charge/discharge profiles. (Reproduced with permission^[70]. Copyright 2020, Wiley-VCH). (E) TEM and HRTEM images of ICS. (F) Band diagram of the ICS. (G) Photocurrent response to UV light. (H) Illustrations of the working principle for the light-induced discharging process. (Reproduced with permission^[82]. Copyright 2020, Wiley-VCH).

In addition, the 2D metal sulfides can also form composites with 1D nanomaterials as promising cathode hosts for Li-CO₂ batteries. For example, Chen *et al.* successfully combined MoS₂/CNT with different ratios serving as a CO₂-cathode electrocatalyst^[77]. Consequently, the ideal MoS₂/CNT realized a maximum discharge capacity (8,551 mAh g⁻¹) with a high coulombic efficiency (96.7%), a charge plateau (3.87 V) at 100 mA g⁻¹ with a limited capacity (500 mAh g⁻¹) and superior electrochemical stability.

2D-3D hybridization

The 2D materials primarily adopt a hierarchical architecture to grow vertically on the 3D substrate surface, promoting electrons to be transported rapidly in the 2D plane^[78-81]. For instance, MnOOH arrays *in-situ* grown on the stainless-steel (SS) network have been reported and employed as a cathode in Li-CO₂ batteries^[20]. Experiments and calculations confirmed that the generation of reaction intermediates (LiCO₂, LiCO and Li₂CO₃) interacting with MnOOH by Li⁺ modulated the formation of Li₂CO₃ and C, promoting their growth on MnOOH uniformly. The ultrafine Li₂CO₃ particles embedded into the carbon substrate significantly enlarge the contact interface, thus promoting the transport of electrons via the discharge products and improving CO₂ evolution activity.

Recently, Guan *et al.* reported a photo-assisted Li-CO₂ battery with a unique characteristic, hierarchical porous and free-supporting In₂S₃@CNT/SS (ICS) as a dual-functional electrode for both CO₂ER and CO₂RR [Figure 7E]^[82]. The 2D In₂S₃ is homogeneously covered on the CNT forest surface, which is helpful to expose abundant active sites and shorten the transport length of photo-holes and photoelectrons [Figure 7F]. Besides, the ICS 2D-3D nanostructure can also promote the rapid transfer of the electron, CO₂, and Li⁺, and expand the electrolyte-electrode contact area. Therefore, the battery showed a high discharge voltage (3.14 V) and ultralow charge voltage (3.20 V), an excellent rate performance and cycle stability, and especially a record superior round trip efficiency (98.1%) [Figure 7G]. These excellent performances can be attributed to the hierarchical porous and self-standing architectures of ICS, and the significant role of photo-assisted electrons and photo-holes during charging-discharging processes [Figure 7H].

ACTIVE SITE ENGINEERING

Defect construction

The utilization of defect engineering has significantly improved the electrochemical performance of various electrochemical energy storage devices^[83]. Among these defect strategies, vacancy is considered a fundamental defect engineering approach for the electronic and geometrical configuration of compounds. For instance, oxygen vacancies (Vo) were introduced into the 2D NiO arrays on the carbon cloth surface (NiO-Vo NAs/CC) using an argon plasma engraving approach^[84]. DFT calculations demonstrated that the Vo causes the appearance of new electronic states near the Fermi level (E_f), resulting in the up-shift of the d-band center. As a result, the NiO-Vo NAs/CC cathode-based Li-CO₂ battery showed higher capacity, more excellent round-trip efficiency, and ultra-long cycle life compared with its counterpart without Vo.

Heteroatom doping of target materials represents another crucial strategy of defect engineering. As an example, Li *et al.* reported vertically aligned N-doped CNT (VA-NCNT) arrays grown on Ti wires free-supporting, binder-free for quasi-solid-state flexible Li-CO₂ batteries^[85]. The VA-NCNT arrays possess a large amount of vertically aligned CNT with high N content, void space and abundant defects, which promote the diffusion of CO₂ and permeation of electrolyte, provide extra space and exposed active sites for the accommodation and generation of Li₂CO₃, and facilitate the dissolution of Li₂CO₃ and amorphous carbon during the charge process.

Recently, Chen *et al.* prepared modified ReS₂ material with a large amount of nucleophilic N dopants and electrophilic S vacancies within its basal plane [Figure 8A]^[86]. The electrophilic and nucleophilic dual centers exhibited suitable adsorption for all intermediates during charge-discharge processes, leading to a low energy barrier in the rate-limiting step. In particular, DEMS measurements confirmed that the mass-to-charge ratios of CO₂ for ReS₂/CP, NS_v-ReS₂(8/7)/CP, and NS_v-ReS₂(5)/CP-based cathodes respectively are 0.63, 0.72, and 0.75 [Figure 8B-D]. Thus, NS_v-ReS₂(5)/CP exhibited a 100% faradic efficiency of 3CO₂/4e⁻ process, having higher CO₂RR activity, while ReS₂/CP cathodes possessed the lowest CO₂RR activity.

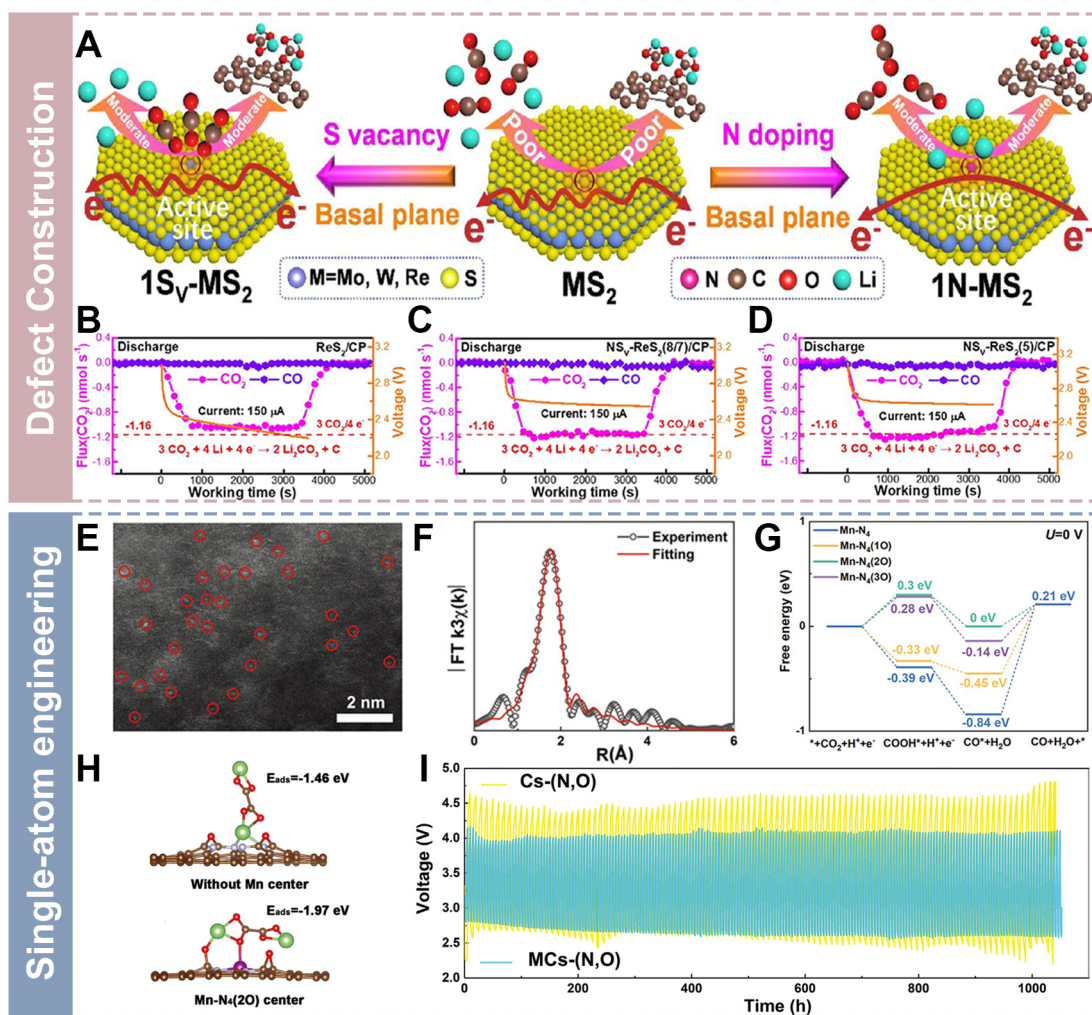


Figure 8. (A) Diagram of the CO₂ER and CO₂RR on the different substrates. DEMS curves with discharge profiles for (B) ReS₂/CP, (C) NSv-ReS₂(8/7)/CP, and (D) NSvReS₂(5)/CP cathodes. (E) The HAADF-STEM image and (F) the fitting EXAFS profiles of MCs- (N, O). (G) Gibbs free energy profiles for the conversion of CO₂ into CO on the different substrates. (H) The adsorption configurations for Li₂C₂O₄ on the various catalysts. (I) Time-voltage curves at 0.02 mA cm⁻². (Reproduced with permission^[86]. Copyright 2021, American Chemical Society). (Reproduced with permission^[95]. Copyright 2023, Wiley-VCH).

Consequently, the optimum catalyst delivered an ultrasmall voltage gap (0.66 V) and ultrahigh energy efficiency (81.1%) at 20 μA cm⁻². The introduction of dual defect centers offers novel opportunities to design excellent bifunctional catalysts of Li-CO₂ batteries.

Single-atom engineering

Among various catalysts, single-atom catalysts (SACs) with quantum size effect, unique coordination structure, and metal-carrier interactions show the advantages of maximized metal utilization, excellent tunability of electrocatalytic sites, and cost-effectiveness. They have been commonly used in many fields such as electrocatalysis, photocatalysis and energy storage devices^[87-90]. Recently, researchers have extended their application to aprotic Li-CO₂ batteries to study their catalytic performance in this emerging field^[91-94].

The well-defined and uniformly dispersed active sites in SACs provide excellent selectivity and activity for electrochemical CO₂ER and CO₂RR in Li-CO₂ batteries^[68]. For example, Mn-N₄ atomic sites [Figure 8E] are

encapsulated into a mesoporous carbon microsphere with the epoxy functional groups by Wang *et al.*^[95]. As a CO₂ electrocatalyst of aprotic Li-CO₂ batteries, the Mn-SACs with N and O-doped electrocatalyst [MCs-(N, O)] with special bowl-like mesoporous morphology and well-regulated active sites optimize the nucleation growth process of discharge products. The *ex-situ* X-ray absorption fine-structure (EXAFS) fitting results indicated that Mn atoms were coordinated with four N atoms [Figure 8F]. DFT calculations demonstrated that an energy barrier of 0.30 eV for Mn-N₄(2O) is significantly lower than other theoretical models of the CO desorption, indicating the better energetics for CO₂ reduction [Figure 8G]. In addition, the optimized model of Mn-N₄(2O) possesses a higher adsorption energy (-1.97 eV) for Li₂C₂O₄ compared with N, O-doped graphene (-1.46 eV) [Figure 8H]. The "surface-adsorption growth pathway" is more favored when the binding energy is higher, leading to the direct formation of a thin layer of Li₂CO₃ products on the CO₂ cathode surface. The results indicated that the Li-CO₂ cell using the MCs-(N, O) cathode can achieve a low voltage gap of about 1.3 V while working stably for 1,000 h [Figure 8I]. In addition to the Mn single atoms mentioned above, transition metal SACs, including Fe, Co, Ni, Cu, Zn, and Cd, have also been reported as high-efficiency electrocatalysts in Li-CO₂ batteries^[94,96-99].

According to a past report, the defective areas on the graphene substrate with a smaller work function and a superior reducing ability could form atomic metal clusters resulting from the electroless deposition of metal ions. In this regard, Xu *et al.* synthesized copper polyphthalocyanine-CNTs composite materials (CuPPc-CNTs) via *in-situ* polymerization of CuPPc on the surface of CNTs as the CO₂ host for reversible Li-CO₂ batteries^[100]. CuPPc possesses very efficient Cu SA electrocatalytic sites with good CO₂ activation and adsorption, while CNTs offer a conductive network. Benefiting from the cooperative effect of the two compounds facilitates Li-CO₂ batteries to achieve excellent discharge capacity (18,652.7 mAh g⁻¹) at 100 mA·g⁻¹ and 1.64 V polarization at a current density of 1,000 mA g⁻¹. Similarly, Zheng proposed molecularly dispersed catalysts [molecularly dispersed electrocatalysts (MDEs)] of nickel phthalocyanine (NiPc) confined on CNTs as the CO₂ electrocatalyst for Li-CO₂ batteries^[93]. The dispersed NiPc efficiently facilitates CO₂ reduction, while the porous and conductive CNT networks promote CO₂ER, leading to improved charging and discharging performance compared with the CNTs and NiPc mixture.

Heterostructure

In order to achieve material multifunctionalities, a kind of common strategy is to prepare chemical composite materials by combining various material components so as to obtain an integration of multifunctional nature. This material design tactic has been widely applied into electrode materials for Li-CO₂ batteries^[67,71,101-103]. For example, a RuAl/Ru heterostructure (RuAl/Ru) material was synthesized by the microstructure and phase reconstruction of a RuAl alloy^[104]. Attributed to multiple benefits of the optimized electronic structure, the multilevel porous structure, and the rich RuAl/Ru interface, RuAl/Ru exhibited much superior stability and electrocatalytic activity than its counterpart. DFT calculations demonstrated the important role of the intrinsically superior activity of RuAl heterointerface to adjust the adsorption of intermediates, thereby reducing the decomposition barrier of the Li-decomposition steps during the CO₂ER.

It is worth noting that the in-built electric field (BEF) based on heterostructure with different Fermi levels has been a highly effective tactic for optimizing interface charge transfer and distribution, thereby adjusting the micro-environment of catalytic sites of catalyst surface and lowering the free energy barriers for the generation of reaction intermediates^[27,105,106]. Lu *et al.* proposed a BEF-driven oriented electron conduction tactic for electrocatalytic redox of CO₂ based on a tandem electrocatalyst, Fe₂O₃@CoS, which is derived from spent lithium-ion batteries [Figure 9A]^[107]. The tandem electrocatalyst exhibited excellent catalytic activities for CO₂ER and CO₂RR in the Li-CO₂ batteries with an extremely high energy efficiency (92.4%), an extremely small voltage gap (0.26 V), and a long cycle life of over 550 h at 20 μA cm⁻². The differential

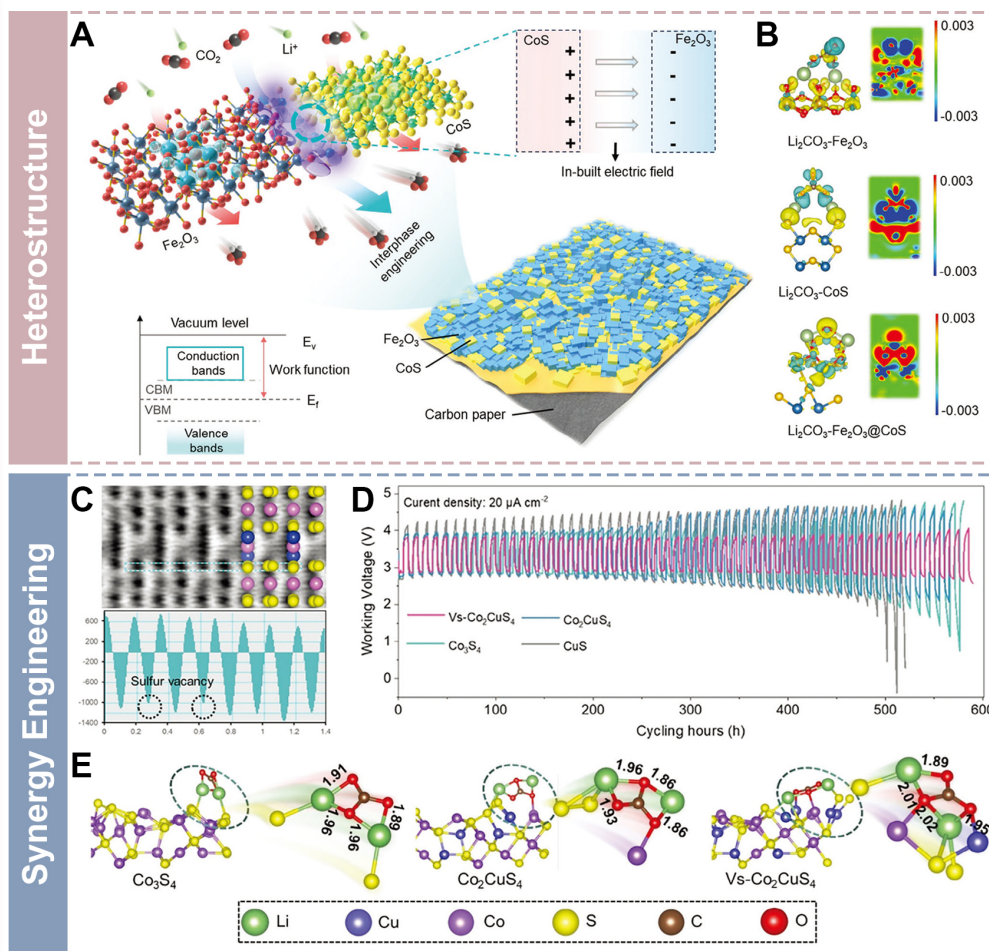


Figure 9. (A) Schematic illustration of the BEF generated on the $\text{Fe}_2\text{O}_3@\text{CoS}$. (B) The charge density difference of different systems. (Reproduced with permission^[107]. Copyright 2023, Wiley-VCH). (C) The double-spherical-aberration-corrected TEM image of $\text{Vs-Co}_2\text{CuS}_4$. (D) Cycling performance of different cathode materials. (E) Adsorption models and Li-O bond length of Li_2CO_3 . (Reproduced with permission^[101]. Copyright 2023, Wiley-VCH).

charge density analysis suggested that Li_2CO_3 adsorbed on the surface of $\text{Fe}_2\text{O}_3@\text{CoS}$ showed more interface electron transfer, inducing more active interactions compared with CoS and Fe_2O_3 [Figure 9B]. The well-defined heterointerface-induced BEF adjusted the adsorption and dissolution of the species during CO_2ER and CO_2RR , empowering the recycled tandem electrocatalyst with remarkable bidirectional catalytic activities.

Synergy engineering

The creation of interacting sites with synergy between multiple active sites is superior to the one with only solo active sites in enhancing Li- CO_2 batteries^[108]. In this regard, incorporating the single atoms into the metal clusters or metal compounds can synergistically enhance the electrocatalytic activity toward CO_2 redox reactions in the Li- CO_2 battery. Lian *et al.* introduced Ru atoms into the Co_3O_4 nanosheet arrays grown on the surface of carbon cloth (SA Ru- $\text{Co}_3\text{O}_4/\text{CC}$), and applied successfully in Li- CO_2 batteries^[65]. The Co_3O_4 nanosheet arrays with 3D structure have a high specific surface area and suitable pore volume/size to promote the mass transfer of reactants and electrolytes, and provide sufficient space to accommodate the discharge products of C and Li_2CO_3 . In addition, uniformly dispersed Ru atoms as active sites regulated

the nucleation process of discharge products, therefore optimizing their ultimate distribution, which is beneficial for redecomposition behavior during the charging process. Lately, Lin *et al.* fabricated a new electrocatalyst comprising well-defined single-atom Ru-N₄ (Ru_{SA}) and atomic clusters (Ru_{AC}) active sites anchored on carbon nanobox substrates (Ru_{SA+AC}@NCB) as electrocatalytic cathodes for Li-CO₂ batteries^[109]. The electronic synergistic effect between Ru_{SA} and Ru_{AC} empowers the Ru_{SA+AC} composite site with enhanced electrocatalytic activity for CO₂RR and CO₂ER in the Li-CO₂ cell, as proved by the much smaller charge/discharge overpotential of the Ru_{SA+AC}@NCB-based cathode than those of the Ru_{AC}@NCB, Ru_{SA}@NCB and NCB-based cathodes.

Very recently, Lu *et al.* found that the tuned p-band and d-band centers of Co₃S₄ by virtue of Cu and S vacancies were hybridized between Li species and CO₂, separately, which is beneficial for the dissolution of Li₂CO₃ and the adsorption of intermediates^[110]. Double-spherical-aberration-corrected transmission electron microscopy (TEM) demonstrated that Cu, S and Co atomic columns are observed clearly [Figure 9C]. The intensity of S active sites in the marked area is obviously lower than that of other active sites, indicating the presence of S vacancies. The Vs-Co₂CuS₄ cathode exhibited outstanding electrochemical performance with an extremely low voltage gap (0.73 V), as well as a lower charge voltage (3.88 V) and a higher discharge voltage (2.73 V) after 600 h of cycling at 20 μA cm⁻² [Figure 9D], which is obviously better than those of CuS, Co₃S₄, Co₂CuS₄ cathodes. The density of states calculation results indicated that compared with Co₂CuS₄ and Co₃S₄, d-band and p-band centers of Vs-Co₂CuS₄ obviously up-shift after the introduction of sulfur vacancies and Cu in Co₃S₄. In addition, the Li-O bond length of Li₂CO₃ adsorbed on the catalyst surface of Vs-Co₂CuS₄ became longer than those of Co₂CuS₄ and Co₃S₄ [Figure 9E]. Thus, when the adsorbed substrate was converted from Co₃S₄ to Vs-Co₂CuS₄ and Co₂CuS₄, the decomposition behavior of Li₂CO₃ became easier. To date, despite the inspiring progress, more efforts still need to be made to explore a better synergistic effect between the electrocatalyst activity and catalytic cathode structure being devoted to achieving excellent battery performance.

Identification and reconstruction of active sites

The identification and reconstruction of the active sites in a working electrocatalyst play a vital role in regulating the catalytic activity and battery reaction kinetics. Considering catalysts with various oxidation states and coordinated configurations, identification of the active reaction sites and their interaction mechanism with the battery reaction is highly required. For example, Liu *et al.* found that Co-O₆ octahedra are the primary active motifs in Co₃O₄^[111]. They utilized an ion-substitution method involving catalytically inert Al³⁺ and Zn²⁺ with d⁰ and d¹⁰ configurations substituting Co ions in octahedral and tetrahedral sites, which Co²⁺_{Td} and Co³⁺_{Oh} retain in synthesized CoAl₂O₄ and ZnCo₂O₄ [Figure 10A]. As a result, the Co₃O₄ showed the highest capacity (2,407 μAh cm⁻² with a high -coulombic efficiency (86.3%). The ZnCo₂O₄ exhibited a capacity (1,995 μAh cm⁻²) with Coulombic efficiencies of 85.6% [Figure 10B]. In contrast, CoAl₂O₄ had nearly no capacity, indicating its inertness in Li-CO₂ batteries. The finite element method (FEM) simulation demonstrated that the majority of the surface of CoAl₂O₄ exhibited sluggish CO₂ transfer ability owing to the obstruction by the large area of Li₂CO₃ product, while the transport ability of Co₃O₄ and ZnCo₂O₄ exhibited faster after discharge [Figure 10C]. Consequently, the high catalytic activity of octahedral Co facilitates uniform and vertical Li₂CO₃ growth during discharge, promoting fast mass transport and charge transfer during battery operation. In contrast, the large Li₂CO₃ particles on the surface of the catalyst, which contains only tetrahedral Co, obstruct the CO₂ diffusion, and therefore, CO₂RR is gradually substituted by Li-ion intercalation reaction during discharge, resulting in a large overpotential [Figure 10D]. Subsequently, DFT calculations indicated that the e_g orbitals in an octahedral structure play a crucial role in CO₂RR activity, in which lower e_g filling and O charge promotes the CO₂ and Li adsorption [Figure 10E].

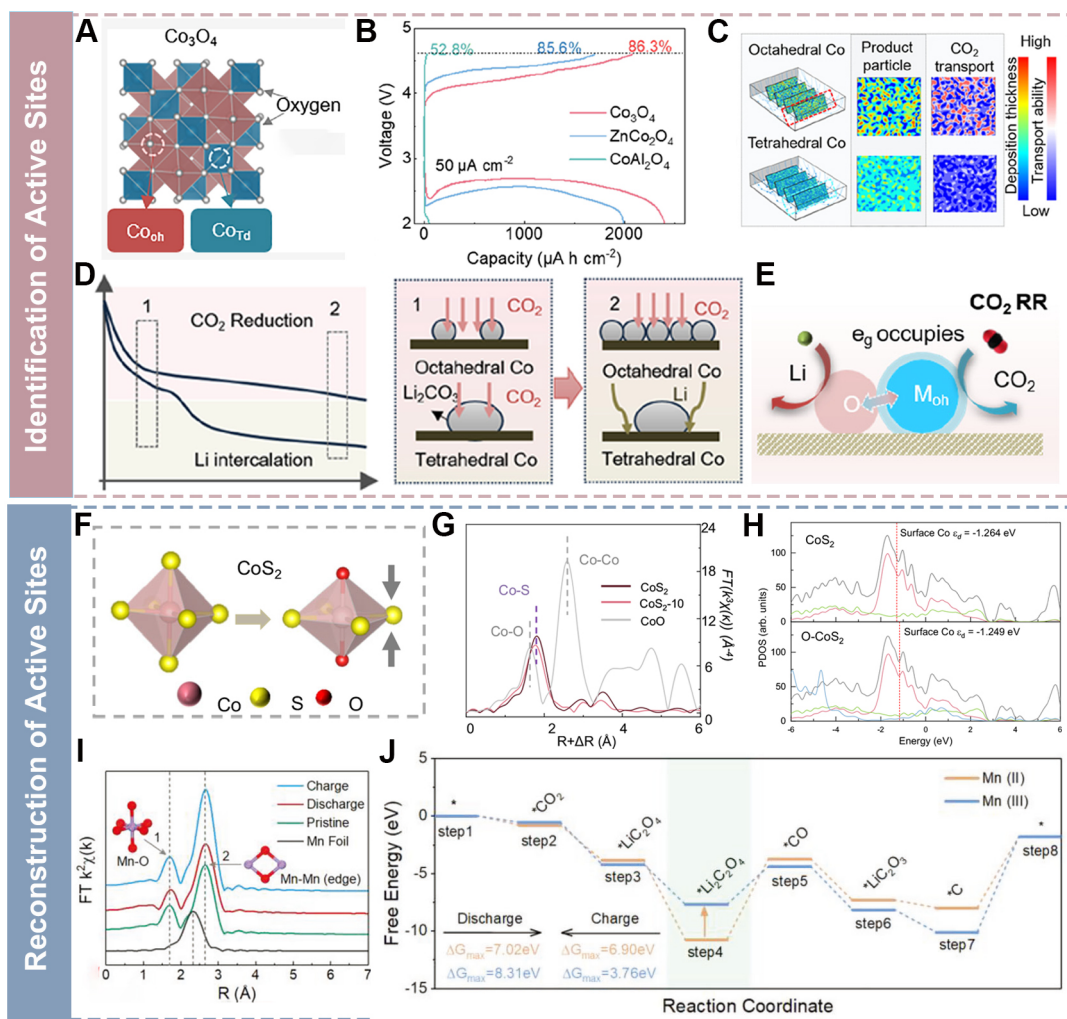


Figure 10. (A) Structure illustration of Co_3O_4 . (B) Galvanostatic charge-discharge profiles of different electrodes. (C) Schematics diagram of the discharge product (Li_2CO_3) generation morphology as well as its impact on CO_2 transport on the different cathode catalysts in the FEM simulation. (D) Schematic illustration of discharge reaction on tetrahedral and octahedral Co. (E) Schematic of the correlation between M-O states and CO_2RR activity. (Reproduced with permission^[111]. Copyright 2024, American Chemical Society). (F) Schematic illustration of structural evolution of CoS_2 . (G) Co K-edge FT-EXAFS of CoS_2 at different stages. (H) The projected density of states (PDOS) of CoS_2 and O- CoS_2 . (Reproduced with permission^[112]. Copyright 2024, Springer Nature). (I) The EXAFS spectra for Mn K-edge. (J) The optimal routes for Mn(II) and Mn(III) sites during discharge and charge processes. (Reproduced with permission^[113]. Copyright 2024, Wiley-VCH).

Compared with transition metal oxide catalysts, metal sulfides exhibit superior electrocatalytic abilities in Li- CO_2 batteries. However, the thermodynamically unstable sulfides are prone to irreversible reconstruction, especially oxidation, due to the aggressive oxygen species resulting from Li_2CO_3 decomposition. Their reconstructed structures and different oxidized states can regulate the activity of sulfides. For instance, Liu *et al.* explored the structural evolution and electrochemical performance of three varieties of cobalt (II) sulfide (CoS_x , $x = 8/9, 1.097$, and 2) pre-electrocatalysts in Li- CO_2 batteries^[112]. X-ray absorption spectroscopy analysis suggested the oxidation of CoS_2 with $\text{Co-S}_4\text{-O}_2$ motifs [Figure 10F and G], while Co_9S_8 and $\text{CoS}_{1.097}$ are completely oxidized to CoO structure in Li- CO_2 batteries. DFT calculations indicated that partial oxygen substitution regulated the electronic structure and moved the d-band center of Co to a higher energy level [Figure 10H], thereby enhancing the catalytic performance of CoS_2 . As a result, reconstructed CoS_2 with $\text{Co-S}_4\text{-O}_2$ motifs exhibited high energy conversion efficiency (> 80%) and excellent

cycling stability with a low overpotential of 0.43 V after 400 h. Recently, Liu *et al.* reported novel Mn dual-active sites (MOC) anchored on N-doped carbon nanofibers^[113]. They observed that MOC underwent significant electrochemical reconstruction during battery cycling due to the *in-situ* formation and stable presence of Mn(III). Mn(III) is reduced to Mn(II) during the discharge process, while Mn(II) was electrochemically oxidized to Mn(III) during subsequent charging process. EXAFS analysis exhibited the intensity and coordination number of Mn-O and Mn-Mn peaks significantly changes during the discharge and charge proceeds, demonstrating the electrochemical reconstruction appearing during CO₂RR and CO₂ER possesses [Figure 10I]. In the charged state, in particular, the peak intensity of the Mn-Mn and MnC/ON enhanced, further revealing the occurrence of Mn(III). DFT calculations exhibited the Gibbs free energy for the charge/discharge processes, indicating that Mn(II) is more advantageous for CO₂RR, while Mn(III) is more conducive for CO₂ER. The crystal occupation Hamiltonian population (COHP) results indicated that the Mn(III) sites possess a more conducive electronic structure for breaking the Li-O bond of the intermediate (*Li₂C₂O₄) during the charging process, thereby facilitating the dissociation of Li₂C₂O₄ and promoting the kinetics of the CO₂ER process [Figure 10J].

CONCLUSIONS AND PERSPECTIVES

In the context of carbon neutralization and carbon peak, the emerging Li-CO₂ battery device has become a facile promising approach, which can trap and recover CO₂ while acting as a power source for sustainable energy networks. In this work, we have systematically summarized recent research progress in the nanostructure design and active site engineering of CO₂ cathode materials for Li-CO₂ batteries, in which the interactions of structures and performance are discussed. Firstly, the working mechanisms of Li-CO₂ batteries with non-aqueous electrolyte are discussed. Next, diverse possible tactics for nanostructures and active site engineering of cathode materials are reviewed in detail. These tactics include morphological regulation, dimensional hybridization, defect construction, single-atom, and heterostructure engineering. Undoubtedly, these strategies have unique advantages for high-performance Li-CO₂ batteries, as summarized in Figure 11 and Table 1. These advances in nanostructure and active-site engineering tactics of CO₂ cathodes in advanced Li-CO₂ batteries have significantly alleviated some vital issues and challenges and promoted the Li-CO₂ battery performances. However, some limitations and problems still need to be solved.

In terms of morphological regulation, first, the applications of nanomaterials with various geometrical shapes in Li-CO₂ batteries have significantly demonstrated their ability to modulate overall properties and, finally, promote electrochemical performance. For example, hollow structure possesses a high surface-to-volume ratio, unique micro-reactor environment, low density, and shortened transport lengths of mass (Li⁺ and CO₂) and charge. However, there are a series of other architectures not reported for Li-CO₂ batteries, such as multilayered hollow spheres and nanorods. The fabrication of nanostructured shapes needs suitable synthetic methods and post-treatment strategies. In addition, the evolution and formation mechanism of nanostructured shapes should be explored. The mechanism comprehension of nucleation and growth principles can effectively regulate the unique morphologies, sizes, and the orientation.

Second, dimension-different nanomaterials usually have different functions and can improve performance from different angles. For instance, the nanofiber networks can provide fast mass transport and charge transfer pathways. The abundant surface of 2D materials significantly alleviates the accumulation of discharge products and enables the maximum electro-contact between the cathode and discharge products, which can effectively reduce the energy threshold to accelerate the decomposition process of discharge products. Meanwhile, their hybridization of diverse forms can combine these functions and benefits flexibly. Nevertheless, the interactions between distinct dimensions of micro/nanostructure have not been well-

Table 1. Summary of electrochemical performance of previous reports on various cathodes in Li-CO₂ batteries

Materials	Rate performance current/capacity (mA g ⁻¹ /mAh g ⁻¹)	Areal capacity (mAh cm ⁻²)	Catalyst loading (mg cm ⁻²)	References
0D Ru	-	1.81	2.2	[54]
Ru @C	20,000/1,000	13.2	0.3	[55]
Holey CNTs	1,000/500	3.15	0.18	[32]
1D Ir-Te	2,000/1,000	-	-	[60]
2D RuRh	-	2.88	0.3	[44]
3D CNT/G	1,000/1,000	6.14	0.35	[81]
2D RuCo ₂ /CNT	500/1,000	1.77	0.22	[37]
Ir NSs-CNFs	500/1,000	2.3	0.3	[80]
VA-NCNT	1,000/1,000	0.37	0.02	[85]
NiO-CNT	100/1,000	-	-	[76]
HOF-Ru@CNT	5,000/1,000	12.12	0.5	[53]
MnTPzP-Mn	200/1,000	6.49	0.36	[47]
Cu-TCPP	2,000/1,000	-	-	[45]
TTCOF-Mn	500/1,000	1.3	0.1	[49]
NiS ₂ /FeS ₂ -N, S-3DG	1,500/1,000	5.3	0.25	[71]
MnO _x -CeO ₂ @PPy	-	15.4	1.13	[59]
Mo ₃ P/Mo	500/500	2.12	0.2	[103]
ZnS QDs/N-rGO	-	4.12	0.4	[67]
RuAl/Ru	2,000/1,000	-	0.8	[104]
Fe-SA/N, S-HG	1,000/1,000	4.87	0.21	[70]
Cd-SA	100,000/1,000	10.4	0.065	[94]
Fe-SA-rGO	-	5.1	0.3	[96]
Ru-NC@rGO	2,000/1,000	8.94	0.2	[91]
NiPc-CN	500/800	2.05	0.19	[93]
Cu-LSCM	1,200/1,000	1.93	0.17	[108]

studied so far. Much effort in the future should be devoted to revealing these inherent relationships and influencing factors. In addition, for the multidimension-hybridized materials, complicated synthesis and time-consuming treatment procedures are not advantageous to their application in energy storage devices. Therefore, it is very significant to utilize simpler and more facile solutions to produce multidimensional-hybridized nanomaterials.

Third, although active site engineering of cathode catalysts significantly improved electrochemical performance of Li-CO₂ batteries, the catalytic performance and structural stability of catalysts may be compromised. For example, excessive defects could lead to the structural degradation or direct decomposition of catalysts. In order to maximize the advantage of engineering effect, the catalytic performance and the structural stability of CO₂ cathode material need to be balanced. Moreover, while synthesizing defects can promote the catalytic active sites for CO₂RR and CO₂ER, the formed coordination-unsaturated atom site near the defects shows ultrahigh redox activity, probably aggravating the parasitic conversion reactions in Li-CO₂ batteries with aprotic electrolyte. In addition, sophisticated active site engineering tactics, such as synergy engineering and heterostructure, still lack rational design principles toward high-performance catalyst cathodes of Li-CO₂ batteries. The heterostructure with some theoretical geometric combinations can be similar to a chaotic system, but its inherent characteristics of abnormal dynamic evolution result in overwhelming research difficulty on its electrochemical performance in Li-CO₂ batteries. It is necessary to investigate structural reconstruction of catalysts and discern the actual active

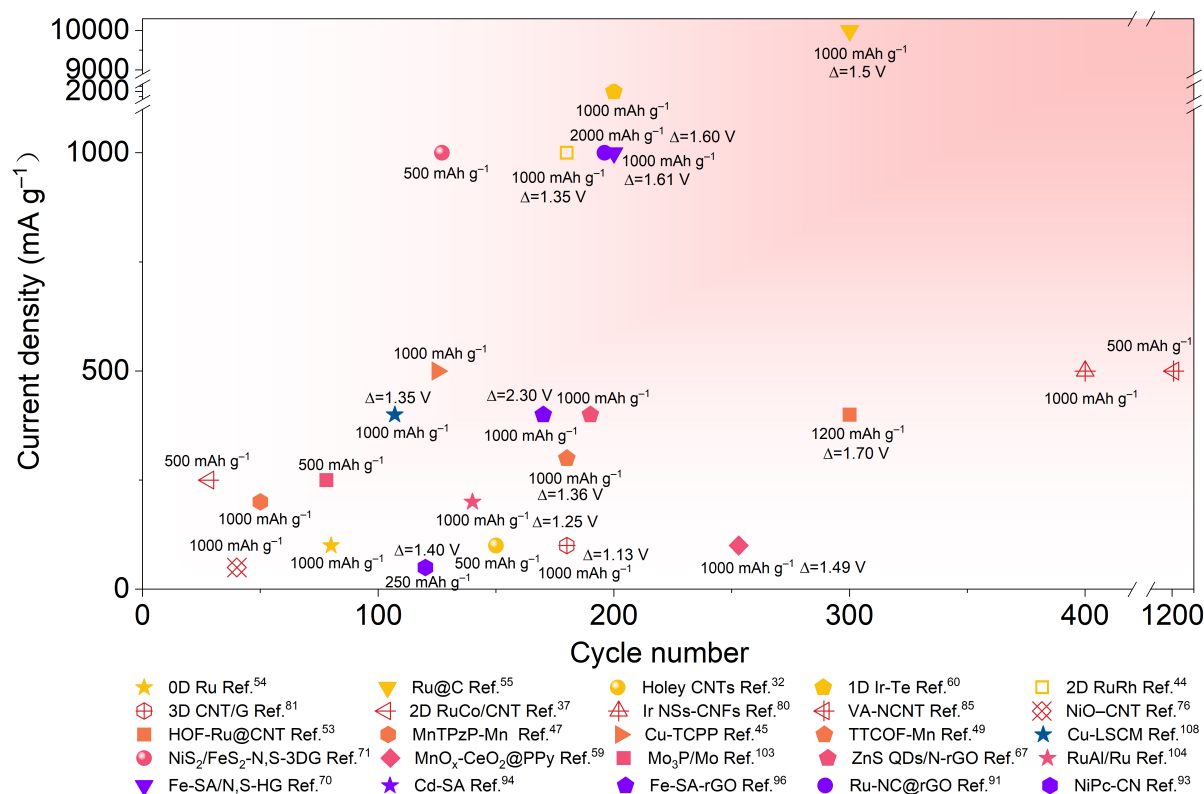


Figure 11. Comparison of cycle number and current density based on previously reported advanced Li-CO₂ battery cathodes.

sites, which will be used to deeply understand active sites and intrinsic characteristics in structural adaptation under cycling processes, promoting the development of advanced electrocatalysts for high-performance Li-CO₂ batteries. Therefore, more attention needs to be given to it. By researching the evolution of atomic or electronic configurations, the advanced *in-situ/operando* characterizations and theoretical calculations could offer valuable information for rational design of electrocatalysts.

Restricted by the inadequate contact between solid-state discharge products and solid catalysts, as well as the passivated active centers on the surface of solid catalysts, soluble catalysts are recognized to enhance cycle life and energy efficiency, particularly effective at decomposing insulating solid reaction products. Generally, an appropriate soluble catalyst to accelerate CO₂ conversion reactions should fulfill the following requirements: (1) high solubility in electrolyte; (2) proper redox potential; (3) reversible redox reaction; and (4) chemical stability to reactive species and electrolyte component. Up to now, several varieties of soluble catalysts have been reported in the Li-CO₂ batteries^[24,114-116]. However, it is noteworthy that the soluble redox mediators that have been employed currently can only meet certain requirements in CO₂RR or CO₂ER process, and whether the redox mediators can promote the deposition of the carbon species in Li₂CO₃ decomposition process remains unknown. Furthermore, the side reactions induced by the addition of redox mediators are also challenged for the anode to realize long cyclability. Consequently, more attention should be focused in this field.

In summary, although some issues are still in the way, the Li-CO₂ systems integrating CO₂ fixation with electrochemical energy storage have been considered as a sustainable and efficient route toward carbon neutralization. We firmly believe that advanced Li-CO₂ batteries will become one of the most practical and

eco-friendly electrochemical energy storage devices through the persistent research of high activity, and stability, as well as low-cost electrocatalysts, stable electrolytes, and the related redox reaction mechanisms in the future.

DECLARATIONS

Authors' contributions

Writing-original draft: Sun, H.; Di, C.; Wu, Z.

Writing-review & editing: Jiang, Y.; Hussain, I.

Conceived and designed manuscript, supervision, and funding acquisition: Ye, Z.

Availability of data and materials

Not applicable.

Financial support and sponsorship

This work was supported by the National Natural Science Foundation of China (52302240), the Macau Young Scholars Program (AM2023011), and the Yuanguang Scholars Program of Hebei University of Technology (282022554).

Conflicts of interest

All authors declared that there are no conflicts of interest.

Ethical approval

Not applicable.

Consent to participate

Not applicable.

Copyright

© The Author(s) 2025.

REFERENCES

1. Nejat, P.; Jomehzadeh, F.; Taheri, M. M.; Gohari, M.; Abd. Majid, M. Z. A global review of energy consumption, CO₂ emissions and policy in the residential sector (with an overview of the top ten CO₂ emitting countries). *Renew. Sustain. Energy. Rev.* **2015**, *43*, 843-62. DOI
2. Li, H.; Du, H.; Luo, H.; Wang, H.; Zhu, W.; Zhou, Y. Recent developments in metal nanocluster-based catalysts for improving photocatalytic CO₂ reduction performance. *Microstructures* **2023**, *3*, 2023024. DOI
3. Zou, J.; Liang, G.; Zhang, F.; Zhang, S.; Davey, K.; Guo, Z. Revisiting the role of discharge products in Li-CO₂ batteries. *Adv. Mater.* **2023**, *35*, e2210671. DOI PubMed
4. Ye, Z.; Jiang, Y.; Li, L.; Wu, F.; Chen, R. Rational design of MOF-based materials for next-generation rechargeable batteries. *Nanomicro. Lett.* **2021**, *13*, 203. DOI PubMed PMC
5. Guo, Y.; Cao, Y.; Lu, J.; Zheng, X.; Deng, Y. The concept, structure, and progress of seawater metal-air batteries. *Microstructures* **2023**, *3*, 2023034. DOI
6. Liang, S.; Zheng, L. J.; Song, L. N.; Wang, X. X.; Tu, W. B.; Xu, J. J. Accelerated confined mass transfer of MoS₂ 1D nanotube in photo-assisted metal-air batteries. *Adv. Mater.* **2024**, *36*, e2307790. DOI PubMed
7. Fetrow, C. J.; Carugati, C.; Zhou, X. D.; Wei, S. Electrochemistry of metal-CO₂ batteries: opportunities and challenges. *Energy. Storage. Mater.* **2022**, *45*, 911-33. DOI
8. Rabiee, H.; Yan, P.; Wang, H.; Zhu, Z.; Ge, L. Electrochemical CO₂ reduction integrated with membrane/adsorption-based CO₂ capture in gas-diffusion electrodes and electrolytes. *EcoEnergy* **2024**, *2*, 3-21. DOI
9. Ahmadi-paridari, A.; Warburton, R. E.; Majidi, L.; et al. A long-cycle-life lithium-CO₂ battery with carbon neutrality. *Adv. Mater.* **2019**, *31*, e1902518. DOI
10. Liu, B.; Sun, Y.; Liu, L.; et al. Recent advances in understanding Li-CO₂ electrochemistry. *Energy. Environ. Sci.* **2019**, *12*, 887-922. DOI

11. Chen, J.; Chen, X. Y.; Liu, Y.; et al. Recent progress of transition metal-based catalysts as cathodes in O₂/H₂O-involved and pure Li-CO₂ batteries. *Energy. Environ. Sci.* **2023**, *16*, 792-829. DOI
12. Takechi, K.; Shiga, T.; Asaoka, T. A Li-O₂/CO₂ battery. *Chem. Commun.* **2011**, *47*, 3463-5. DOI PubMed
13. Xu, S.; Das, S. K.; Archer, L. A. The Li-CO₂ battery: a novel method for CO₂ capture and utilization. *RSC. Adv.* **2013**, *3*, 6656. DOI
14. Liu, F.; Zhou, J.; Wang, Y.; et al. Rational engineering of 2D materials as advanced catalyst cathodes for high-performance metal-carbon dioxide batteries. *Small. Struct.* **2023**, *4*, 2300025. DOI
15. Ma, Z.; Yuan, X.; Li, L.; et al. A review of cathode materials and structures for rechargeable lithium-air batteries. *Energy. Environ. Sci.* **2015**, *8*, 2144-98. DOI
16. Zhang, Z.; Xiao, X.; Zhu, X.; Tan, P. Addressing transport issues in non-aqueous Li-air batteries to achieving high electrochemical performance. *Electrochem. Energy. Rev.* **2023**, *6*, 157. DOI
17. Zhang, Z.; Xiao, X.; Yan, A.; Sun, K.; Yu, J.; Tan, P. A quantitative understanding of electron and mass transport coupling in lithium-oxygen batteries. *Adv. Energy. Mater.* **2023**, *13*, 2302816. DOI
18. Goodarzi, M.; Nazari, F.; Illas, F. Assessing the performance of cobalt phthalocyanine nanoflakes as molecular catalysts for Li-promoted oxalate formation in Li-CO₂-oxalate batteries. *J. Phys. Chem. C.* **2018**, *122*, 25776-84. DOI
19. Németh, K.; Srajer, G. CO₂/oxalate cathodes as safe and efficient alternatives in high energy density metal-air type rechargeable batteries. *RSC. Adv.* **2014**, *4*, 1879-85. DOI
20. Ma, S.; Lu, Y.; Yao, H.; Si, Y.; Liu, Q.; Li, Z. Regulating the nucleation of Li₂CO₃ and C by anchoring Li-containing carbonaceous species towards high performance Li-CO₂ batteries. *J. Energy. Chem.* **2022**, *65*, 472-9. DOI
21. Qiao, Y.; Yi, J.; Wu, S.; et al. Li-CO₂ electrochemistry: a new strategy for CO₂ fixation and energy storage. *Joule* **2017**, *1*, 359-70. DOI
22. Angamuthu, R.; Byers, P.; Lutz, M.; Spek, A. L.; Bouwman, E. Electrocatalytic CO₂ conversion to oxalate by a copper complex. *Science* **2010**, *327*, 313-5. DOI PubMed
23. Ye, Z.; Sun, H.; Gao, H.; et al. Intrinsic activity regulation of metal chalcogenide electrocatalysts for lithium-sulfur batteries. *Energy. Storage. Mater.* **2023**, *60*, 102855. DOI
24. Li, W.; Zhang, M.; Sun, X.; et al. Boosting a practical Li-CO₂ battery through dimerization reaction based on solid redox mediator. *Nat. Commun.* **2024**, *15*, 803. DOI PubMed PMC
25. Wang, Y. F.; Song, L. N.; Zheng, L. J.; Wang, Y.; Wu, J. Y.; Xu, J. J. Reversible carbon dioxide/lithium oxalate regulation toward advanced aprotic lithium carbon dioxide battery. *Angew. Chem. Int. Ed.* **2024**, *63*, e202400132. DOI
26. Zhao, Z.; Su, Y.; Peng, Z. Probing lithium carbonate formation in trace-O₂-assisted aprotic Li-CO₂ batteries using in situ surface-enhanced Raman spectroscopy. *J. Phys. Chem. Lett.* **2019**, *10*, 322-8. DOI
27. Xue, H.; Gong, H.; Lu, X.; et al. Aqueous formate-based Li-CO₂ battery with low charge overpotential and high working voltage. *Adv. Energy. Mater.* **2021**, *11*, 2101630. DOI
28. Zhang, F.; Co, A. C. Direct evidence of local pH change and the role of alkali cation during CO₂ electroreduction in aqueous media. *Angew. Chem. Int. Ed.* **2020**, *59*, 1674-81. DOI PubMed
29. Hou, Y.; Wang, J.; Liu, L.; et al. Mo₂C/CNT: an efficient catalyst for rechargeable Li-CO₂ batteries. *Adv. Funct. Mater.* **2017**, *27*, 1700564. DOI
30. Tang, Z.; Yuan, M.; Zhu, H.; et al. Promoting the performance of Li-CO₂ batteries via constructing three-dimensional interconnected K⁺ doped MnO₂ nanowires networks. *Front. Chem.* **2021**, *9*, 670612. DOI PubMed PMC
31. Pipes, R.; He, J.; Bhargav, A.; Manthiram, A. Freestanding vanadium nitride nanowire membrane as an efficient, carbon-free gas diffusion cathode for Li-CO₂ batteries. *Energy. Storage. Mater.* **2020**, *31*, 95-104. DOI
32. Xie, H.; Zhang, B.; Hu, C.; Xiao, N.; Liu, D. Boosting Li-CO₂ battery performances by creating holey structure on CNT cathodes. *Electrochim. Acta.* **2022**, *417*, 140310. DOI
33. Qi, G.; Zhang, J.; Chen, L.; Wang, B.; Cheng, J. Binder-free MoN nanofibers catalysts for flexible 2-electron oxalate-based Li-CO₂ batteries with high energy efficiency. *Adv. Funct. Mater.* **2022**, *32*, 2112501. DOI
34. Chen, Y.; Fan, Z.; Wang, J.; et al. Ethylene selectivity in electrocatalytic CO₂ reduction on Cu nanomaterials: a crystal phase-dependent study. *J. Am. Chem. Soc.* **2020**, *142*, 12760-6. DOI
35. Zhou, J.; Wang, T.; Chen, L.; et al. Boosting the reaction kinetics in aprotic lithium-carbon dioxide batteries with unconventional phase metal nanomaterials. *Proc. Natl. Acad. Sci. USA.* **2022**, *119*, e2204666119. DOI PubMed PMC
36. Guo, L.; Tan, L.; Xu, A.; et al. Highly efficient two-dimensional Ag₂Te cathode catalyst featuring a layer structure derived catalytic anisotropy in lithium-oxygen batteries. *Energy. Storage. Mater.* **2022**, *50*, 96-104. DOI
37. Wang, Y.; Zhou, J.; Lin, C.; et al. Decreasing the overpotential of aprotic Li-CO₂ batteries with the in-plane alloy structure in ultrathin 2D Ru-based nanosheets. *Adv. Funct. Mater.* **2022**, *32*, 2202737. DOI
38. Fan, L.; Shen, H.; Ji, D.; et al. Biaxially compressive strain in Ni/Ru core/shell nanoplates boosts Li-CO₂ batteries. *Adv. Mater.* **2022**, *34*, e2204134. DOI
39. Zhao, W.; Yang, Y.; Deng, Q.; et al. Toward an understanding of bimetallic MXene solid-solution in binder-free electrocatalyst cathode for advanced Li-CO₂ batteries. *Adv. Funct. Mater.* **2023**, *33*, 2210037. DOI
40. Yu, W.; Shen, Z.; Yoshii, T.; et al. Hierarchically porous and minimally stacked graphene cathodes for high-performance lithium-oxygen batteries. *Adv. Energy. Mater.* **2024**, *14*, 2303055. DOI
41. Zhou, X.; Zhang, A.; Chen, B.; et al. Synthesis of 2H/fcc-heterophase AuCu nanostructures for highly efficient electrochemical CO₂

- Reduction at industrial current densities. *Adv. Mater.* **2023**, *35*, e2304414. DOI
42. Pipes, R.; He, J.; Bhargav, A.; Manthiram, A. Efficient Li-CO₂ batteries with molybdenum disulfide nanosheets on carbon nanotubes as a catalyst. *ACS Appl. Energy Mater.* **2019**, *2*, 8685-94. DOI
 43. Jiang, C.; Zhang, Y.; Zhang, M.; et al. Exfoliation of covalent organic frameworks into MnO₂-loaded ultrathin nanosheets as efficient cathode catalysts for Li-CO₂ batteries. *Cell. Rep. Phys. Sci.* **2021**, *2*, 100392. DOI
 44. Xing, Y.; Wang, K.; Li, N.; et al. Ultrathin RuRh alloy nanosheets enable high-performance lithium-CO₂ battery. *Matter* **2020**, *2*, 1494-508. DOI
 45. Xu, Y.; Gong, H.; Ren, H.; et al. Highly efficient Cu-porphyrin-based metal-organic framework nanosheet as cathode for high-rate Li-CO₂ battery. *Small* **2022**, *18*, e2203917. DOI
 46. Dong, L. Z.; Zhang, Y.; Lu, Y. F.; et al. A well-defined dual Mn-site based metal-organic framework to promote CO₂ reduction/evolution in Li-CO₂ batteries. *Chem. Commun.* **2021**, *57*, 8937-40. DOI
 47. Li, S.; Dong, Y.; Zhou, J.; et al. Carbon dioxide in the cage: manganese metal-organic frameworks for high performance CO₂ electrodes in Li-CO₂ batteries. *Energy Environ. Sci.* **2018**, *11*, 1318-25. DOI
 48. Wang, J. H.; Li, S.; Chen, Y.; et al. Phthalocyanine based metal-organic framework ultrathin nanosheet for efficient photocathode toward light-assisted Li-CO₂ battery. *Adv. Funct. Mater.* **2022**, *32*, 2210259. DOI
 49. Zhang, Y.; Zhong, R. L.; Lu, M.; et al. Single metal site and versatile transfer channel merged into covalent organic frameworks facilitate high-performance Li-CO₂ batteries. *ACS Cent. Sci.* **2021**, *7*, 175-82. DOI PubMed PMC
 50. Huang, S.; Chen, D.; Meng, C.; et al. CO₂ Nanoenrichment and nanoconfinement in cage of imine covalent organic frameworks for high-performance CO₂ cathodes in Li-CO₂ batteries. *Small* **2019**, *15*, e1904830. DOI
 51. Li, X.; Wang, H.; Chen, Z.; et al. Covalent-organic-framework-based Li-CO₂ batteries. *Adv. Mater.* **2019**, *31*, e1905879. DOI
 52. Chen, Y.; Li, X. Y.; Chen, Z.; et al. Efficient multicarbon formation in acidic CO₂ reduction via tandem electrocatalysis. *Nat. Nanotechnol.* **2024**, *19*, 311-8. DOI
 53. Cheng, Z.; Fang, Y.; Yang, Y.; et al. Hydrogen-bonded organic framework to upgrade cycling stability and rate capability of Li-CO₂ batteries. *Angew. Chem. Int. Ed.* **2023**, *62*, e202311480. DOI
 54. Yang, S.; Qiao, Y.; He, P.; et al. A reversible lithium-CO₂ battery with Ru nanoparticles as a cathode catalyst. *Energy Environ. Sci.* **2017**, *10*, 972-8. DOI
 55. Baek, K.; Jeon, W. C.; Woo, S.; et al. Synergistic effect of quinary molten salts and ruthenium catalyst for high-power-density lithium-carbon dioxide cell. *Nat. Commun.* **2020**, *11*, 456. DOI PubMed PMC
 56. Zhang, K.; Li, J.; Zhai, W.; et al. Boosting cycling stability and rate capability of Li-CO₂ batteries via synergistic photoelectric effect and plasmonic interaction. *Angew. Chem. Int. Ed.* **2022**, *61*, e202201718. DOI
 57. Wang, Z.; Liu, B.; Yang, X.; et al. Dual catalytic sites of alloying effect bloom CO₂ catalytic conversion for highly stable Li-CO₂ battery. *Adv. Funct. Mater.* **2023**, *33*, 2213931. DOI
 58. Cheng, Z.; Wu, Z.; Chen, J.; et al. Mo₃N-ZrO₂ heterostructure engineering in freestanding carbon nanofibers for upgrading cycling stability and energy efficiency of Li-CO₂ batteries. *Small* **2023**, *19*, e2301685. DOI
 59. Deng, Q.; Yang, Y.; Mao, C.; et al. Electronic state modulation and reaction pathway regulation on necklace-like MnO_x-CeO₂@polypyrrole hierarchical cathode for advanced and flexible Li-CO₂ batteries. *Adv. Energy Mater.* **2022**, *12*, 2103667. DOI
 60. Zhai, Y.; Tong, H.; Deng, J.; et al. Super-assembled atomic Ir catalysts on Te substrates with synergistic catalytic capability for Li-CO₂ batteries. *Energy Storage Mater.* **2021**, *43*, 391-401. DOI
 61. Zhang, X.; Wang, T.; Yang, Y.; et al. Breaking the stable triangle of carbonate via W-O bonds for Li-CO₂ batteries with low polarization. *ACS Energy Lett.* **2021**, *6*, 3503-10. DOI
 62. Ye, Z.; Jiang, Y.; Yang, T.; Li, L.; Wu, F.; Chen, R. Engineering catalytic CoSe-ZnSe heterojunctions anchored on graphene aerogels for bidirectional sulfur conversion reactions. *Adv. Sci.* **2022**, *9*, e2103456. DOI PubMed PMC
 63. Ye, Z.; Jiang, Y.; Li, L.; Wu, F.; Chen, R. Self-assembly of 0D-2D heterostructure electrocatalyst from MOF and MXene for boosted lithium polysulfide conversion reaction. *Adv. Mater.* **2021**, *33*, e2101204. DOI
 64. Jiang, Y.; Wu, F.; Ye, Z.; et al. Confining CoTe₂-ZnTe heterostructures on petal-like nitrogen-doped carbon for fast and robust sodium storage. *Chem. Eng. J.* **2023**, *451*, 138430. DOI
 65. Lian, Z.; Lu, Y.; Wang, C.; et al. Single-atom Ru implanted on Co₃O₄ nanosheets as efficient dual-catalyst for Li-CO₂ batteries. *Adv. Sci.* **2021**, *8*, e2102550. DOI PubMed PMC
 66. Hao, Y.; Jiang, Y.; Zhao, L.; et al. Bimetallic antimony-vanadium oxide nanoparticles embedded in graphene for stable lithium and sodium storage. *ACS Appl. Mater. Interfaces.* **2021**, *13*, 21127-37. DOI
 67. Wang, H.; Xie, K.; You, Y.; et al. Realizing interfacial electronic interaction within ZnS quantum Dots/N-rGO heterostructures for efficient Li-CO₂ batteries. *Adv. Energy Mater.* **2019**, *9*, 1901806. DOI
 68. Wang, K.; Liu, D.; Liu, L.; et al. Isolated metalloidal tellurium atomic cluster on nitrogen-doped carbon nanosheet for high-capacity rechargeable lithium-CO₂ battery. *Adv. Sci.* **2023**, *10*, e2205959. DOI PubMed PMC
 69. Jiang, Y.; Wu, F.; Ye, Z.; et al. Superimposed effect of hollow carbon polyhedron and interconnected graphene network to achieve CoTe₂ anode for fast and ultralong sodium storage. *J. Power. Sources.* **2023**, *554*, 232174. DOI
 70. Hu, C.; Gong, L.; Xiao, Y.; et al. High-performance, long-life, rechargeable Li-CO₂ batteries based on a 3D holey graphene cathode implanted with single iron atoms. *Adv. Mater.* **2020**, *32*, e1907436. DOI
 71. Jin, Y.; Liu, Y.; Song, L.; et al. Interfacial engineering in hollow NiS₂/FeS₂-NSGA heterostructures with efficient catalytic activity for

- advanced Li-CO₂ battery. *Chem. Eng. J.* **2022**, *430*, 133029. DOI
72. Liu, Y.; Zhao, S.; Wang, D.; et al. Toward an understanding of the reversible Li-CO₂ batteries over metal-N₄-functionalized graphene electrocatalysts. *ACS. Nano.* **2022**, *16*, 1523-32. DOI
73. Guo, C.; Zhang, F.; Han, X.; et al. Intrinsic descriptor guided noble metal cathode design for Li-CO₂ battery. *Adv. Mater.* **2023**, *35*, e2302325. DOI
74. Liu, L.; Qin, Y.; Wang, K.; et al. Rational design of nanostructured metal/C interface in 3D self-supporting cellulose carbon aerogel facilitating high-performance Li-CO₂ batteries. *Adv. Energy. Mater.* **2022**, *12*, 2103681. DOI
75. Ye, Z.; Jiang, Y.; Li, L.; Wu, F.; Chen, R. Enhanced catalytic conversion of polysulfide using 1D CoTe and 2D MXene for heat-resistant and lean-electrolyte Li-S batteries. *Chem. Eng. J.* **2022**, *430*, 132734. DOI
76. Zhang, X.; Wang, C.; Li, H.; et al. High performance Li-CO₂ batteries with NiO-CNT cathodes. *J. Mater. Chem. A.* **2018**, *6*, 2792-6. DOI
77. Chen, C. J.; Huang, C. S.; Huang, Y. C.; et al. Catalytically active site identification of molybdenum disulfide as gas cathode in a nonaqueous Li-CO₂ battery. *ACS. Appl. Mater. Interfaces.* **2021**, *13*, 6156-67. DOI
78. Liu, W.; Zhai, P.; Li, A.; et al. Electrochemical CO₂ reduction to ethylene by ultrathin CuO nanoplate arrays. *Nat. Commun.* **2022**, *13*, 1877. DOI PubMed PMC
79. Liu, Q.; Hu, Z.; Li, L.; et al. Facile synthesis of birnessite δ-MnO₂ and carbon nanotube composites as effective catalysts for Li-CO₂ batteries. *ACS. Appl. Mater. Interfaces.* **2021**, *13*, 16585-93. DOI
80. Xing, Y.; Yang, Y.; Li, D.; et al. Crumpled Ir nanosheets fully covered on porous carbon nanofibers for long-life rechargeable lithium-CO₂ batteries. *Adv. Mater.* **2018**, *30*, e1803124. DOI
81. Xiao, Y.; Du, F.; Hu, C.; et al. High-performance Li-CO₂ batteries from free-standing, binder-free, bifunctional three-dimensional carbon catalysts. *ACS. Energy. Lett.* **2020**, *5*, 916-21. DOI
82. Guan, D. H.; Wang, X. X.; Li, M. L.; et al. Light/electricity energy conversion and storage for a hierarchical porous In₂S₃@CNT/SS cathode towards a flexible Li-CO₂ battery. *Angew. Chem. Int. Ed.* **2020**, *59*, 19518-24. DOI
83. Shi, Z.; Li, M.; Sun, J.; Chen, Z. Defect engineering for expediting Li-S chemistry: strategies, mechanisms, and perspectives. *Adv. Energy. Mater.* **2021**, *11*, 2100332. DOI
84. Wang, C.; Lu, Y.; Lu, S.; et al. Boosting Li-CO₂ battery performances by engineering oxygen vacancy on NiO nanosheets array. *J. Power. Sources.* **2021**, *495*, 229782. DOI
85. Li, X.; Zhang, J.; Qi, G.; Cheng, J.; Wang, B. Vertically aligned N-doped carbon nanotubes arrays as efficient binder-free catalysts for flexible Li-CO₂ batteries. *Energy. Storage. Mater.* **2021**, *35*, 148-56. DOI
86. Chen, B.; Wang, D.; Tan, J.; et al. Designing electrophilic and nucleophilic dual centers in the ReS₂ plane toward efficient bifunctional catalysts for Li-CO₂ batteries. *J. Am. Chem. Soc.* **2022**, *144*, 3106-16. DOI
87. Wang, Y.; Chu, F.; Zeng, J.; et al. Single atom catalysts for fuel cells and rechargeable batteries: principles, advances, and opportunities. *ACS. Nano.* **2021**, *15*, 210-39. DOI
88. Zhou, A. W.; Wang, D. S.; Li, Y. D. Hollow microstructural regulation of single-atom catalysts for optimized electrocatalytic performance. *Microstructures* **2022**, *2*, 2022005. DOI
89. Zhong, D. C.; Gong, Y. N.; Zhang, C.; Lu, T. B. Dinuclear metal synergistic catalysis for energy conversion. *Chem. Soc. Rev.* **2023**, *52*, 3170-214. DOI PubMed
90. Liu, H.; Li, J.; Arbiol, J.; Yang, B.; Tang, P. Catalytic reactivity descriptors of metal-nitrogen-doped carbon catalysts for electrocatalysis. *EcoEnergy* **2023**, *1*, 154-85. DOI
91. Cheng, J.; Bai, Y.; Lian, Y.; et al. Homogenizing Li₂CO₃ nucleation and growth through high-density single-atomic Ru loading toward reversible Li-CO₂ reaction. *ACS. Appl. Mater. Interfaces.* **2022**, *14*, 18561-9. DOI
92. Rho, Y. J.; Kim, B.; Shin, K.; Henkelman, G.; Ryu, W. H. Atomically miniaturized bi-phase IrO_x/Ir catalysts loaded on N-doped carbon nanotubes for high-performance Li-CO₂ batteries. *J. Mater. Chem. A.* **2022**, *10*, 19710-21. DOI
93. Zheng, H.; Li, H.; Zhang, Z.; et al. Dispersed nickel phthalocyanine molecules on carbon nanotubes as cathode catalysts for Li-CO₂ batteries. *Small* **2023**, *19*, e2302768. DOI
94. Zhu, K.; Li, X.; Choi, J.; et al. Single-atom cadmium-N₄ sites for rechargeable Li-CO₂ batteries with high capacity and ultra-long lifetime. *Adv. Funct. Mater.* **2023**, *33*, 2213841. DOI
95. Wang, M.; Yao, Y.; Tian, Y.; et al. Atomically dispersed manganese on carbon substrate for aqueous and aprotic CO₂ electrochemical reduction. *Adv. Mater.* **2023**, *35*, e2210658. DOI
96. Zhou, L.; Wang, H.; Zhang, K.; et al. Fast decomposition of Li₂CO₃/C actuated by single-atom catalysts for Li-CO₂ batteries. *Sci. China. Mater.* **2021**, *64*, 2139-47. DOI
97. Ding, J.; Xue, H.; Xiao, R.; et al. Atomically dispersed Fe-N_x species within a porous carbon framework: an efficient catalyst for Li-CO₂ batteries. *Nanoscale* **2022**, *14*, 4511-8. DOI
98. Shi, Y.; Wei, B.; Legut, D.; Du, S.; Francisco, J. S.; Zhang, R. Highly stable single-atom modified MXenes as cathode-active bifunctional catalysts in Li-CO₂ battery. *Adv. Funct. Mater.* **2022**, *32*, 2210218. DOI
99. Xu, Y.; Gong, H.; Song, L.; et al. A highly efficient and free-standing copper single atoms anchored nitrogen-doped carbon nanofiber cathode toward reliable Li-CO₂ batteries. *Mater. Today. Energy.* **2022**, *25*, 100967. DOI
100. Xu, Y.; Jiang, C.; Gong, H.; et al. Single atom site conjugated copper polyphthalocyanine assisted carbon nanotubes as cathode for reversible Li-CO₂ batteries. *Nano. Res.* **2022**, *15*, 4100-7. DOI

101. Li, J.; Zhang, K.; Zhao, Y.; et al. High-efficiency and stable Li-CO₂ battery enabled by carbon nanotube/carbon nitride heterostructured photocathode. *Angew. Chem. Int. Ed.* **2022**, *61*, e202114612. DOI
102. Deng, Q.; Yang, Y.; Yin, K.; Yi, J.; Zhou, Y.; Zhang, Y. Boosting active species Ru-O-Zr/Ce construction at the interface of phase-transformed zirconia-ceria isomerism toward advanced catalytic cathodes for Li-CO₂ batteries. *Adv. Energy. Mater.* **2023**, *13*, 2302398. DOI
103. Wu, C.; Qi, G.; Zhang, J.; Cheng, J.; Wang, B. Porous Mo₃P/Mo nanorods as efficient mott-schottky cathode catalysts for low polarization Li-CO₂ battery. *Small* **2023**, *19*, e2302078. DOI
104. Jian, T.; Ma, W.; Hou, J.; Ma, J.; Xu, C.; Liu, H. From Ru to RuAl intermetallic/Ru heterojunction: enabling high reversibility of the CO₂ redox reaction in Li-CO₂ battery based on lowered interface thermodynamic energy barrier. *Nano. Energy.* **2023**, *118*, 108998. DOI
105. Zhang, P. F.; Zhang, J. Y.; Sheng, T.; et al. Synergetic effect of Ru and NiO in the electrocatalytic decomposition of Li₂CO₃ to enhance the performance of a Li-CO₂/O₂ battery. *ACS. Catal.* **2020**, *10*, 1640-51. DOI
106. Hao, Y.; Hu, F.; Zhu, S.; et al. MXene-regulated metal-oxide interfaces with modified intermediate configurations realizing nearly 100% CO₂ electrocatalytic conversion. *Angew. Chem. Int. Ed.* **2023**, *62*, e202304179. DOI
107. Lu, B.; Min, Z.; Xiao, X.; et al. Recycled tandem catalysts promising ultralow overpotential Li-CO₂ batteries. *Adv. Mater.* **2024**, *36*, e2309264. DOI
108. Zou, L.; Li, R.; Wang, Z.; Yu, F.; Chi, B.; Pu, J. Synergistic effect of Cu-La_{0.96}Sr_{0.04}Cu_{0.3}Mn_{0.7}O_{3-δ} heterostructure and oxygen vacancy engineering for high-performance Li-CO₂ batteries. *Electrochim. Acta.* **2021**, *395*, 139209. DOI
109. Lin, J.; Ding, J.; Wang, H.; et al. Boosting energy efficiency and stability of Li-CO₂ battery via synergy between Ru atom cluster and single atom Ru-N₄ site in electrocatalyst cathode. *Adv. Mater.* **2022**, *34*, 2200559. DOI
110. Lu, B.; Wu, X.; Xiao, X.; et al. Energy band engineering guided design of bidirectional catalyst for reversible Li-CO₂ batteries. *Adv. Mater.* **2024**, *36*, e2308889. DOI
111. Liu, Y.; Shu, P.; Zhang, M.; et al. Uncovering the geometry activity of spinel oxides in Li-CO₂ battery reactions. *ACS. Energy. Lett.* **2024**, *9*, 2173-81. DOI
112. Liu, Y.; Zhang, Z.; Tan, J.; et al. Deciphering the contributing motifs of reconstructed cobalt (II) sulfides catalysts in Li-CO₂ batteries. *Nat. Commun.* **2024**, *15*, 2167. DOI PubMed PMC
113. Liu, L.; Shen, S.; Zhao, N.; et al. Revealing the indispensable role of in situ electrochemically reconstructed Mn(II)/Mn(III) in improving the performance of lithium-carbon dioxide batteries. *Adv. Mater.* **2024**, *36*, e2403229. DOI
114. Khurram, A.; He, M.; Gallant, B. M. Tailoring the discharge reaction in Li-CO₂ batteries through incorporation of CO₂ capture chemistry. *Joule* **2018**, *2*, 2649-66. DOI
115. Wang, X. G.; Wang, C.; Xie, Z.; et al. Improving electrochemical performances of rechargeable Li-CO₂ batteries with an electrolyte redox mediator. *ChemElectroChem* **2017**, *4*, 2145-9. DOI
116. Pipes, R.; Bhargav, A.; Manthiram, A. Phenyl disulfide additive for solution-mediated carbon dioxide utilization in Li-CO₂ batteries. *Adv. Energy. Mater.* **2019**, *9*, 1900453. DOI